NASA Technical Memorandum 83300

THREE-DIMENSIONAL ANALYSIS OF $[0/90]_s$ AND $[90/0]_s$ LAMINATES WITH A CENTRAL CIRCULAR HOLE

Ivatury S. Raju and John H. Crews, Jr.

April 1982

NASA
National Aeronautics and
Space Administration

Langley Research Center
Hampton, Virginia 23665

THREE-DIMENSIONAL ANALYSIS OF $[0/90]_s$ AND $[90/0]_s$ LAMINATES WITH A CENTRAL CIRCULAR HOLE

Ivatury S. Raju* and John H. Crews, Jr.**
NASA Langley Research Center
Hampton, Virginia 23665

SUMMARY

Stress distributions were calculated near a circular hole in $[0/90]_s$ and $[90/0]_s$ laminates, using a three-dimensional finite-element analysis. These stress distributions were presented three ways: through the thickness at the hole boundary, along radial lines at the 0/90 and 90/0 interfaces, and around the hole at these interfaces. The interlaminar normal stress, σ_z, and the shear stress, $\sigma_{z\theta}$, distributions had very steep gradients near the hole boundary, suggesting interlaminar stress singularities. The largest compressive σ_z stress occurred at about 60° from the load axis; the largest $\sigma_{z\theta}$ occurred near 75°. A simple procedure was introduced to calculate interlaminar stresses near the hole boundary. It used stresses calculated by an exact two-dimensional analysis of a laminate with a hole as input to a quasi-three-dimensional model. It produced stresses that agreed closely with those from the three-dimensional finite-element model. For laminates with holes, this simple procedure may become a viable alternative to three-dimensional finite-element analyses.

---

*Assistant Research Professor, Joint Institute for Advancement of Flight Sciences, George Washington University at NASA Langley Research Center.

**Senior Engineer.

INTRODUCTION

Composite laminates are being used extensively in aerospace structures. Many such laminates develop high interlaminar stresses near holes; such stresses can cause delamination. Unfortunately, the stress state near a circular hole in a laminate is a complex three-dimensional (3-D) problem. The only exact solutions to the problems are two-dimensional (2-D) [1]. The literature contains little work on 3-D problems. Dana and Barker [2] used the finite-element method to analyze the stresses around circular holes in $[0/90]_s$, $[90/0]_s$, and $[\pm 45]_s$ laminates; they used very coarse models, however. Experience with a less complex straight-edge problem [3] showed that coarse models may not yield accurate results near the interlaminar stress singularity that can exist at the hole boundary. Tang [4] used a boundary-layer theory to obtain stress distributions around a circular hole in $[0/90]_s$ and $[\pm 45]_s$ laminates, but he used an extremely large value of 400 for the ratio of hole radius to ply thickness.

One purpose of this paper is to present accurate 3-D stresses for a composite laminate with a more representative ratio of hole radius to the ply thickness. A second purpose is to introduce a method for estimating the major interlaminar stresses near a circular hole. The present paper does not present design information; instead, it addresses the basic understanding of 3-D stresses at a laminate hole.

The present study focused on four-ply laminates with $[0/90]_s$ and $[90/0]_s$ stacking sequences. A central circular hole of radius equal to 20 times the ply thickness was considered. The laminate had a length-to-width ratio of two, and the width was six times the hole diameter. A laminate of such dimensions

is, effectively, infinitely wide and long relative to the hole diameter. This laminate was analyzed by a finite-element method, like that in Ref. 3, with very high mesh refinement near the intersection of the interface between plies and the hole boundary.

The stress distributions are presented in three ways: through the thickness, along radial lines away from the hole, and around the hole. Because an interlaminar stress singularity was expected between the 0° and 90° plies at the hole, the computed stresses were given very near but not at the hole boundary. Furthermore, the stress magnitudes very near this singularity may depend on finite-element mesh refinement. As a result, the peak stresses near the hole were used only for relative comparisons at different locations around the hole and for relative comparisons among the 3-D stress components at specific points.

SYMBOLS

E_{ii}	Young's modulus in i-direction, MPa
G_{ij}	shear modulus, MPa
h	ply thickness, m
L	half-length of the laminate, m
R	radius of the circular hole, m
r,θ	polar coordinates
S_g	gross-section stress, MPa
u,v,w	displacements in x-, y-, and z-direction, respectively, m
W	half-width of the laminate, m
x,y,z	Cartesian coordinates, m
ν_{ij}	Poisson's ratios

$\{\sigma\}$ cylindrical stresses σ_r, σ_θ, σ_z, $\sigma_{r\theta}$, $\sigma_{\theta z}$, σ_{zr}, MPa

$\{\varepsilon\}$ cylindrical strains ε_r, ε_θ, ε_z, $\varepsilon_{r\theta}$, $\varepsilon_{\theta z}$, ε_{zr}

Subscripts

i,j i,j = 1,2,3

1,2,3 longitudinal, transverse, and thickness directions of a ply

ANALYSIS

This section describes the problem analyzed and the corresponding finite-element model.

Laminated Composite Plate with a Circular Hole

Fig. 1 shows a four-ply laminate with a half-length of 240h, half-width of 120h, and half-thickness of 2h. It has a central circular hole with a radius of 20h. The ends of the laminate were subjected to a uniform displacement in the x-direction. The gross-section stress necessary for this deformation was S_g.

As previously mentioned, two laminates, $[0/90]_s$ and $[90/0]_s$, were considered in the analyses. Each ply was idealized as a homogeneous, elastic, orthotropic material with the same properties as in Refs. 3, 5, 6, and 7.

$$E_{11} = 138 \text{ GPa } (20 \times 10^6 \text{ psi})$$

$$E_{22} = E_{33} = 14.5 \text{ GPa } (2.1 \times 10^6 \text{ psi})$$

$$G_{12} = G_{23} = G_{31} = 5.86 \text{ GPa } (0.85 \times 10^6 \text{ psi})$$

$$\nu_{12} = \nu_{13} = \nu_{23} = 0.21$$

The subscripts 1, 2, and 3 denote the longitudinal, transverse, and thickness directions, respectively, of an individual ply.

The analysis is aimed at obtaining the stress distribution in the idealized laminate due to the above-mentioned loading, S_g. Because of the complexity in satisfying the equations of equilibrium, compatibility conditions, and boundary conditions of orthotropic elasticity, exact solutions are not available. Therefore, approximate methods are being used to obtain the stress distributions in the laminate. In the present study, a finite-element analysis based on displacement formulation was used.

Because of the symmetries in the problem, only one-eighth of the laminate was analyzed, as shown in Fig. 1. The displacements u, v, and w were prescribed as zero on $x = 0$, $y = 0$, and $z = 0$ planes, respectively. On the $x = 240h$ plane, a constant displacement $u = u_o$ was prescribed. The gross-section stress S_g necessary for this deformation was $302u_o/h$, MPa.

To facilititate presentation of results, a cylindrical coordinate system (r,θ,z) was also used. The stresses in the cylindrical system are shown in Fig. 1.

Finite-Element Idealization

One-eighth of the laminate ($0 \leq x \leq 240h$, $0 \leq y \leq 120h$, and $0 \leq z \leq 2h$) was modeled by 20-node isoparametric brick elements. The plan view of the model is shown in Fig. 2(a) and a 20-noded brick element is shown in Fig. 2(b).

The model was subdivided into three regions: a 2-D region, a transition region, and a 3-D region. The unshaded region in Fig. 2(a) corresponds to the 2-D region. The shaded region very near the hole corresponds to the transition and the 3-D regions.

Fig. 3 shows the through-the-thickness modeling typical of the nine radial lines shown in Fig. 2(a). The 3-D region extended from $20h$ to $26h$, the

transition was in the region 26h to 27h, and the 2-D region was from 27h onward. In the 3-D region very near the hole ($20h \leq r \leq 21h$ and $0 \leq z \leq 2h$), a polar-type arrangement of elements was used. The polar mesh had a very fine arrangement of elements very near the hole. This arrangement yields a concentration of stress values very near the intersection of the interface and the hole ($z = h$, $r = R$), where a stress singularity is expected. A very similar polar mesh was used in Ref. 3 for a quasi-three-dimensional analysis of the straight-edge problem in a laminate.

The 2-D region extends outward from $r = 27h$ (see Fig. 3). This 2-D region was also modeled by 20-node isoparametric brick elements. In this region, one element per ply was used through the thickness and the displacements were assumed to be independent of z. For example, nodes i, j, and k in Fig. 3 had identical u, v, and w displacements. Furthermore, the constitutive relations for the elements in the 2-D region were edited to produce plane stress $(\sigma_z = 0)$ conditions. Thus, the 20-node isoparametric brick elements degenerated to 8-node plane stress quadrilateral elements.

The transition elements provided compatibility between the 3-D and 2-D regions. The transition elements were developed like those reported in Ref. 8.

The element sizes used in the present finite-element modeling are an order of magnitude smaller than the fiber diameters used in current graphite/epoxy laminates. Even so, the present analysis was not aimed at idealizing the fibers and matrix separately, but was aimed at analyzing laminates idealized as consisting of homogeneous, orthotropic plies. Similar assumptions were also used in Refs. 2 and 4.

EVALUATION OF THE FINITE-ELEMENT MODEL

The finite-element model for a θ = constant plane is presented in Fig. 3. The polar arrangement of elements is much like that used in Ref. 3 to analyze a straight-edge problem involving the same material properties and stacking sequences as the present problem. Refs. 3 and 7 show that such a polar mesh gives accurate stresses even near a singularity. Therefore, the present through-the-thickness modeling was expected to be accurate near the interlaminar singularity.

The modeling around the hole was evaluated by comparing 2-D stress distributions with a known exact solution [1]. Because of the polar arrangement of elements, the inplane modeling at the midplane ($z = 0$) and the top surface ($z = 2h$) was identical and was coarser than the inplane modeling at the interface ($z = h$) (see Fig. 3). The inplane modeling at the midplane was used in the 2-D finite-element analysis of a $[0/90]_s$ (or $[90/0]_s$) laminate with a hole.

Fig. 4 shows the hoop stress $\left(\sigma_\theta/S_g\right)$ distribution on the three radial lines, $\theta = 0°$, 45°, and 90°. The distance from the hole is nondimensionalized with the ply thickness. The solid curves represent 2-D (midplane mesh) results and the dashed curves represent the exact 2-D solution for an infinite laminate [1]. The two solutions agree closely along all three radial lines. The exact hoop stress σ_θ has a maximum at $\theta = 90°$ and the corresponding stress-concentration factor, K_T, for an infinite laminate is 4.87. For the present finite-element model, the finite width and length elevate the K_T by about 2.4 percent [9]. Therefore, the exact K_T for the present model is about 4.99. The finite-element solution gave a K_T of 4.92, which

is only 1.4 percent below the exact value. Therefore, even the relatively coarse midplane modeling predicted the stress distributions accurately.

The next parameter to be checked was the extent of the 3-D region. The quasi-3-D analyses in the literature [3, 5, 6, and 7] show that the 3-D stresses die away within a distance of about 4h from a straight free edge. For the present free-hole problem, two different 3-D models were considered. One model had 3-D elements extending to a distance 6h from the hole (from 20h to 26h), as shown previously in Fig. 3. The second model had a smaller 3-D region, extending to 4h (i.e., from 20h to 24h) from the hole. The 3-D stresses from both models were nearly identical, showing that either model was adequate. The model with the larger 3-D region ($20h \leq r \leq 26h$) was used throughout the remainder of this study. This model had about 19,000 degrees of freedom.

Because the finite-element idealization shown in Figs. 2 and 3 can account for the through-the-thickness variations, inplane variations, and 3-D effects, the model was considered accurate and was used to study the stress distribution in the $[0/90]_s$ and $[90/0]_s$ laminates with a central circular hole.

RESULTS AND DISCUSSION

As previously mentioned, stresses are presented first as through-the-thickness distributions, next as radial distributions at the interface, and then as circumferential distributions at the interface. Lastly, estimated interlaminar stresses based on a procedure described in the Appendix are compared with stresses from the 3-D hole model. The results for the $[0/90]_s$ and $[90/0]_s$ laminates are presented and discussed together.

Through-the-Thickness Distributions

Hoop Stress, σ_θ--Figs. 5(a) and 5(b) show the σ_θ distributions through the thickness at the hole boundary ($r/R = 1$) for the $[0/90]_s$ and $[90/0]_s$ laminates, respectively. For comparison, stresses from the 2-D exact solution for an infinite plate [1] are shown as dashed lines. These 2-D stresses are, by assumption, uniform through each ply. The hoop stress, σ_θ, at $\theta = 90°$ in the 0° plies of both laminates shows the largest variation. The gradient of σ_θ in these plies is sharpest near the interface ($z/h = 1$). This "peak" is probably caused by an interlaminar stress singularity at the interface [3]. Although the present finite-element method yields accurate stresses very near singularities, it cannot calculate stresses at such singularities [7]. For this reason, the stress results from the two elements closest to each side of the interface were neglected, as in Ref. 7. Because these elements were within the narrow range $0.998 \leq z/h \leq 1.002$, their absence is not noticeable in Fig. 5. (These two elements were also neglected in all subsequent through-the-thickness plots.) In general, the σ_θ peaks for $\theta = 0°$ and 45° in Fig. 5 were quite small. Results for the two laminates were similar and also agreed reasonably well with the exact 2-D solution.

Interlaminar Normal Stress, σ_z--Figs. 6(a) and 6(b) show σ_z through the thickness at the $\theta = 0°$, 45°, and 90° angular locations on the hole boundary at the $[0/90]_s$ laminate. At all three locations, the curves have steep gradients near the interface. These results strongly suggest the existence of interlaminar stress singularities at the hole boundary. Furthermore, at $\theta = 0°$ and 90° the σ_z stresses are discontinuous across the interface ($z = h$). Similar behavior was observed in Refs. 3 and 6. However, the present discontinuities may be somewhat magnified because the σ_z stresses were not plotted for the two elements on either side of the interface, as previously discussed. Near the

midplane the σ_z distributions have smooth gradients and show no evidence of a stress singularity. The interfacial σ_z is compressive at $\theta = 0°$ and 45° and tensile at $\theta = 90°$. At the midplane, however, the σ_z is tensile at $\theta = 45°$ and compressive at $\theta = 0°$ and 90°.

Figs. 6(c) and 6(d) show σ_z through the thickness for the $[90/0]_s$ laminate. As in the $[0/90]_s$ case, the distributions near the interface show steep gradients and discontinuities, suggesting interlaminar stress singularities at the hole boundary. The interfacial σ_z is compressive at $\theta = 0°$ and 45° and tensile at $\theta = 90°$, as in the $[0/90]_s$ case, but with slightly different magnitudes. At the midplane, in contrast to the $[0/90]_s$ case, the σ_z is tensile only at $\theta = 90°$.

Interlaminar Shear Stress, $\sigma_{z\theta}$--Figs. 7(a) and 7(b) present the $\sigma_{z\theta}$ distributions through the thickness. Distributions are presented only for $\theta = 45°$ because $\sigma_{z\theta}$ is identically zero at $\theta = 0°$ and 90°, which are planes of symmetry. The two distributions are similar but of opposite sign. This can be explained because the load transfers from the 0° top ply to the midply in the $[0/90]_s$ case, while in the $[90/0]_s$ case the load transfers from the 0° midply to the top ply. Both laminates show steep gradients near the interface, again suggesting a stress singularity.

Radial Distributions

The radial distributions for interlaminar stresses σ_z, $\sigma_{z\theta}$, and σ_{zr} are presented at three angular positions, $\theta = 0°$, 45°, and 90°.

Interlaminar Normal Stress, σ_z--Figs. 8(a) and 8(b) show the interlaminar σ_z distributions away from the hole for $[0/90]_s$ and $[90/0]_s$ laminates, respectively. In these figures, and as in Fig. 4, the stresses are plotted against

$(r - R)/h$, the distance from the hole in terms of the ply thickness h. The interlaminar stresses from the two elements closest to the hole boundary were neglected because of the possible singularity there. Beyond these two elements ($(r - R)/h \geq 0.002$), the σ_z discontinuities across the interface were small, only about 2 percent of that shown in Fig. 6(b) for the hole boundary. Therefore, the interlaminar σ_z values were calculated by averaging the 0° and 90° ply values at the interface, a customary finite-element practice.

The σ_z distributions for the $[0/90]_s$ laminate (Fig. 8(a)) have steep gradients very close to the hole boundary. The largest value of σ_z occurred at $\theta = 45°$ and is about 15 percent of the gross section stress, S_g. At all three locations, σ_z switches sign very near the hole boundary. Furthermore, for larger values of $(r - R)/h$, the σ_z becomes vanishingly small, with σ_z at $\theta = 0°$ showing the most rapid decay to zero.

Fig. 8(b) shows that the σ_z distributions for the $[90/0]_s$ laminate are somewhat similar to the $[0/90]_s$ case. However, in contrast to the $[0/90]_s$ case, the σ_z curves for $\theta = 45°$ and 90° do not switch signs near the hole boundary. Also, they become vanishingly small within one ply thickness from the hole.

Interlaminar Shear Stress, $\sigma_{z\theta}$--Figs. 9(a) and 9(b) show the radial variation of $\sigma_{z\theta}$ for $[0/90]_s$ and $[90/0]_s$ laminates, respectively. On the planes of symmetry $\theta = 0°$ and 90°, $\sigma_{z\theta}$ is zero. The $\sigma_{z\theta}$ curves have very steep gradients close to the hole boundary, suggesting the presence of a singularity there. At two elements away ($(r - R)/h = 0.002$) from the boundary, the $\sigma_{z\theta}$ was about 60 percent as large as S_g. The two distributions in Figs. 9(a) and 9(b) are identical except for their signs. This sign difference was expected, as discussed in the previous section.

Interlaminar Shear Stress, σ_{zr}--Figs. 10(a) and 10(b) show the radial variation of interlaminar σ_{zr} distributions. In both figures the σ_{zr} curves for $\theta = 0°$ and $90°$ do not approach zero at the hole boundary, as might be expected. On the hole boundary, of course, the corresponding complementary stress σ_{rz} should be zero because this boundary is to be stress free. This apparent discrepancy can be explained by the presence of an interlaminar stress singularity at the hole boundary. As shown in Ref. 7, a shear stress and its complement (e.g., σ_{zr} and σ_{rz}) need not be equal at a stress singularity.

Circumferential Distributions

This section presents the circumferential distributions for σ_θ, σ_z, and $\sigma_{z\theta}$ near the hole boundary. Again the stresses from the two elements closest to the hole were neglected. Therefore, the stresses shown closest to the hole are at $r/R = 1.0001$, that is, at a distance of $0.002h$ from the hole boundary.

Hoop Stress, σ_θ--Fig. 11 shows the σ_θ distribution around the hole for both laminates. In this figure ply-thickness average values of σ_θ are plotted for each ply. The ply stresses calculated from the 2-D exact solution are included for comparison. The ply-thickness average σ_θ in the 0° ply agrees very well with the exact solution in the region $0° \leq \theta \leq 45°$. Similar agreement is shown for the 90° ply in the region $45° \leq \theta \leq 90°$. The largest difference between the two solutions was about 15 percent.

Interlaminar Normal Stress, σ_z--Fig. 12 presents the interlaminar σ_z distribution around the hole. The symbols in this figure are stress estimates that will be discussed in the next section. For the $[0/90]_s$ laminate (Fig. 12(a)), σ_z is compressive for most of the region along the hole boundary. The stress is tensile only in the regions $10° \leq \theta \leq 28°$ and $80° \leq \theta \leq 90°$. Its largest compressive value occurs around $\theta = 60°$.

For the $[90/0]_s$ laminate (Fig. 12(b)), σ_z is again compressive for most of the region around the hole, with a small tensile region near $\theta = 90°$. The largest compressive value occurs near $\theta = 60°$.

Interlaminar Shear Stress, $\sigma_{z\theta}$--The interlaminar $\sigma_{z\theta}$ distributions around the hole are shown in Figs. 13(a) and 13(b). Again, the symbols are estimates to be discussed in the next section. Except for different signs, the $\sigma_{z\theta}$ distributions are identical for the two laminates (compare Figs. 13(a) and 13(b)). These distributions both have their largest values at about 75° from the load axis. This suggests that the $\sigma_{z\theta}$ stress singularity is probably strongest near $\theta = 75°$. Also, the largest $\sigma_{z\theta}$ value in Fig. 13 is about 1.65 S_g, which is about 10 times as large as the largest σ_z or σ_{zr} value computed for the same distance ($r/R = 1.0001$) from the hole. This comparison suggests that the $\sigma_{z\theta}$ stress singularity is stronger than those for the σ_z and σ_{zr} interlaminar stresses.

Quasi-3-D Estimates

As mentioned earlier, the interlaminar σ_z and $\sigma_{z\theta}$ stresses were also estimated using the quasi-3-D procedure described in the Appendix. This procedure was based on the assumption that the curved hole boundary could be approximated by a series of straight-edge specimens. Each such segment was analyzed by a quasi-3-D method from the literature (e.g., see Ref. 3). The tangential strain ε_θ in each segment was calculated from the exact 2-D solution for a laminate hole, as presented in Ref. 1. As explained in the Appendix, this ε_θ strain was applied to the straight-edge segment in two different ways. For the simpler case, the ε_θ value at the hole boundary was applied uniformly across the width (radial direction) of each segment. For the

more refined second case, each segment was subjected to the nonuniform radial distribution of ε_θ obtained from the exact 2-D solution in Ref. 1.

Interlaminar Normal Stress, σ_z--The symbols in Fig. 12 show the σ_z estimates at 15° intervals along the hole boundary. The square symbols represent the results from the uniform ε_θ approach and the circular symbols represent the nonuniform ε_θ approach. For the $[0/90]_s$ laminate (Fig. 12(a)), these two approaches estimate the σ_z values very well except at $\theta = 90°$, with both approaches giving very nearly the same values. This leads to the conclusion that the radial gradient of the ε_θ distribution (see the Appendix and Fig. 15) had very little influence on the results. For the $[90/0]_s$ laminate (Fig. 12(b)), the estimates are also very good. The small discrepancies between the estimates and the 3-D finite-element values may be caused by the strain gradients in the θ-direction which were not accounted for by the straight-edge analyses.

Interlaminar Shear Stress, $\sigma_{z\theta}$--Fig. 13 presents the $\sigma_{z\theta}$ estimates. For both laminates the predictions are in excellent agreement with the 3-D values; only the peak value at $\theta = 75°$ was overestimated. Again, both the uniform and nonuniform strain approaches yielded nearly identical values. This suggests that the ε_θ gradients away from the hole in the nonuniform approach had very little influence on the estimates and that the simpler uniform ε_θ approach can be used to estimate σ_z and $\sigma_{z\theta}$ around the hole.

Through-the-thickness and radial distributions of σ_z and $\sigma_{z\theta}$ were also estimated using the quasi-3-D procedure. Unfortunately, the agreement between these estimates and the corresponding 3-D results was not as good as that shown in Figs. 12 and 13. The quasi-3-D procedure needs further evaluation, but this is beyond the scope of the present study.

CONCLUDING REMARKS

Stress distributions were calculated in $[0/90]_s$ and $[90/0]_s$ laminates with a central circular hole, using a three-dimensional finite-element analysis. The laminate was idealized using 20-node isoparametric brick elements. The stress distributions were presented in three ways: through the thickness at the hole boundary, along radial lines at the interface, and around the hole at the interface.

The interlaminar normal stress σ_z and shear stress $\sigma_{z\theta}$ between the 0/90 and 90/0 plies showed very steep gradients very near the hole boundary. These results suggest that an interlaminar stress singularity exists at the hole boundary. For both $[0/90]_s$ and $[90/0]_s$ laminates, the calculated interlaminar stresses were similar, with only minor differences.

The σ_z singularity appears to be strongest at about 60° from the load axis. But this interlaminar σ_z was compressive over most of the region around the hole. The $\sigma_{z\theta}$ singularity appears to be strongest at about 75° from the load axis, and it appears to be stronger than either the σ_z or σ_{zr} singularities. The $\sigma_{z\theta}$ stresses calculated very near the hole boundary were about 10 times the corresponding σ_z and σ_{zr} values.

A simple procedure was proposed to estimate σ_z and $\sigma_{z\theta}$ at the interface very near the hole boundary. This procedure was based on a quasi-three-dimensional straight-edge model, subjected to the tangential hole-boundary strain computed from an exact 2-D analysis. The estimates agreed very well with the computed 3-D stresses. Furthermore, these σ_z and $\sigma_{z\theta}$ interlaminar stresses appear to be governed by the tangential strain value at the hole boundary, rather than its radial distribution.

The simple procedure introduced in this paper appears to be an attractive and economical method for estimating the interlaminar stresses very near holes in composite laminates. This simple procedure may prove to be a viable alternative to a complete three-dimensional analysis of a laminated plate containing a hole. However, the range of applicability of this procedure needs to be checked for more complex laminates than those studied in this paper.

APPENDIX

STRAIGHT-EDGE APPROXIMATION FOR A LAMINATE WITH A HOLE

The purpose of this Appendix is to describe a simplified quasi-3-D procedure to obtain σ_z and $\sigma_{z\theta}$ values very near the hole boundary (r/R = 1.0001 in the present analysis).

Fig. 14 shows one-eighth of the laminate from Fig. 1. The hole boundary was approximated by seven discrete edge segments as shown. Each of these seven segments was analyzed as though it were a laminate with a straight free edge, using the quasi-3-D procedure described in Refs. 3, 5, and 6. According to this procedure, each edge segment was analyzed using a finite-element model for the plane normal to the edge. As shown schematically in Fig. 14, such straight-edge finite-element models were in radial planes at 15° intervals around the hole. These straight-edge models, which are like the model shown earlier in Fig. 3, are described in detail in Ref. 3.

For the $[0/90]_s$ laminates with a hole, the following stacking sequences were used in the straight-edge models: $[90/0]_s$, $[75/-15]_s$, $[60/-30]_s$, $[\pm 45]_s$, $[30/-60]_s$, $[15/-75]_s$, and $[0/90]_s$. These seven stacking sequences may be expressed concisely as $[(90 - \theta)/-\theta]_s$, where θ is measured from the x-axis. For the $[90/0]_s$ laminate with a hole, the corresponding expression is $[-\theta/(90 - \theta)]_s$. These stacking sequences were also used in the straight-edge analyses in Ref. 3.

As shown schematically in Fig. 14, a quasi-3-D, straight-edge model is subjected to a strain normal to the plane of the model. For the present models in radial planes, this strain corresponds to the tangential strains ε_θ around the laminate hole. The tangential strains ε_θ along radial planes were

computed using the 2-D exact solution of Ref. 1. These ε_θ distributions are shown in Fig. 15.

Two different approaches were used for the strain inputs in the quasi-3-D analyses. In the first approach, a uniform ε_θ was imposed. The uniform strain equaled the ε_θ value at the hole boundary. (For example, for the 90° radial plane, a uniform ε_θ of 4.39×10^{-7} was used.) In the second approach, nonuniform distributions of ε_θ from Fig. 15 were imposed, as shown schematically in Fig. 14.

The interlaminar stresses σ_z and $\sigma_{z\theta}$ were computed (at $r/R = 1.0001$) for each radial plane with both uniform and nonuniform ε_θ distributions as inputs. The results from these quasi-3-D analyses are presented in Figs. 12 and 13.

REFERENCES

1. S. G. Lekhnitskii, Theory of Elasticity of an Anisotropic Elastic Body (Holden-Day, Inc., San Francisco, 1963).

2. J. R. Dana and R. M. Barker, "Three-Dimensional Analysis for the Stress Distribution Near Circular Holes in Laminated Composites," VPI&SU Report VPI-E-74-18 (1974).

3. I. S. Raju and J. H. Crews, Jr., "Interlaminar Stress Singularities at a Straight Free Edge in Composite Laminates," J. of Computers and Structures 14(1-2), 21 (1981). (Also available as NASA TM-81876, 1980.)

4. S. Tang, "Interlaminar Stresses Around Circular Cutouts in Composite Plates Under Tension," AIAA Journal 15(1), 1631 (1977).

5. R. B. Pipes and N. J. Pagano, "Interlaminar Stresses in Composite Laminates Under Uniform Axial Extension," J. Comp. Materials 4(4), 538 (1970).

6. A. S. D. Wang and F. W. Crossman, "Some New Results on Edge Effects in Symmetric Composite Laminates," J. Comp. Materials 11(1), 92 (1977).

7. I. S. Raju, J. D. Whitcomb, and J. G. Goree, "A New Look at Numerical Analyses of Free-Edge Stresses in Composite Laminates," NASA TP-1751 (1980).

8. A. V. Krishna Murty and K. N. Shivakumar, "Combined Use of Solid of Revolution, Thin Shell, and Interphase Elements for Analysis of Cylindrical Shells," J. Struct. Mechanics 8(1), 43 (1980).

9. C. S. Hong and J. H. Crews, Jr., "Stress-Concentration Factors for Finite Orthotropic Laminates with a Circular Hole and Uniaxial Loading," NASA TP-1469 (1979).

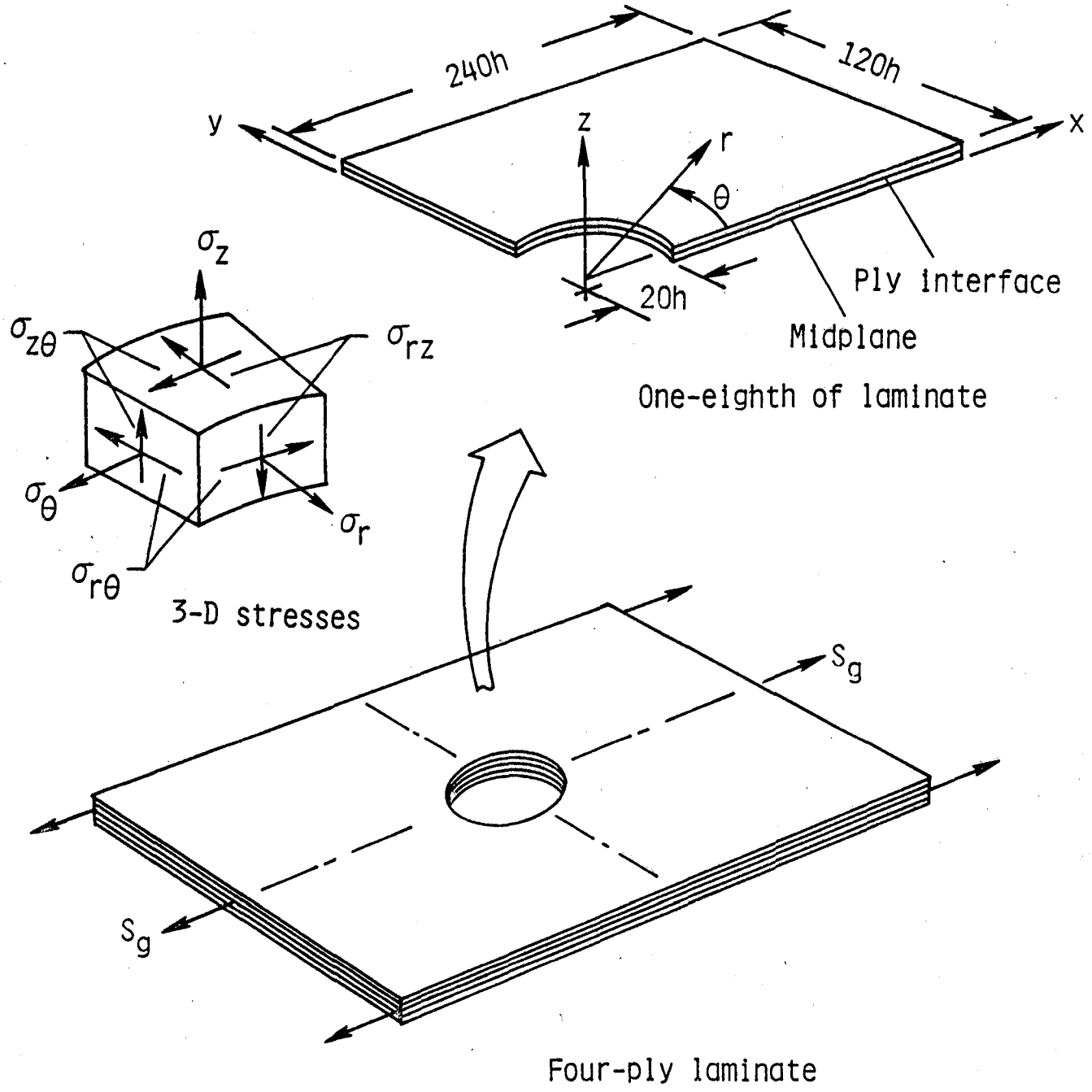

Figure 1.- Laminate configuration, loading, and stresses.

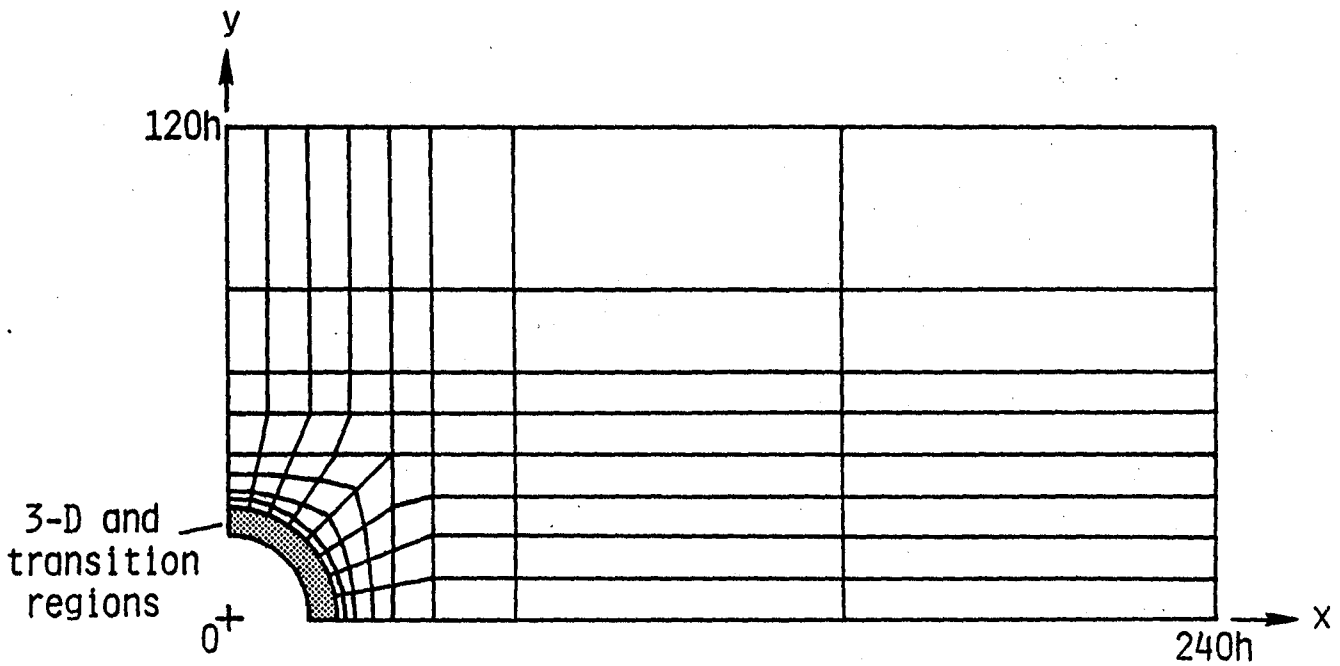

(a) Plan view of finite-element model.

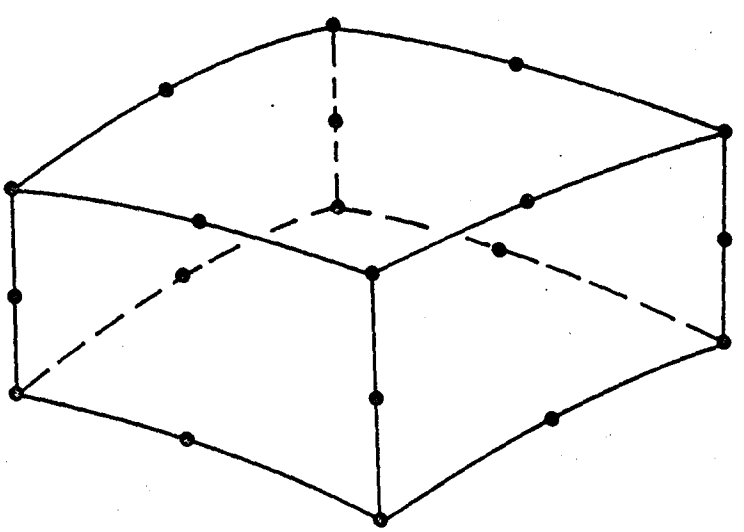

(b) 20-noded isoparametric element.

Figure 2.- Finite element and model.

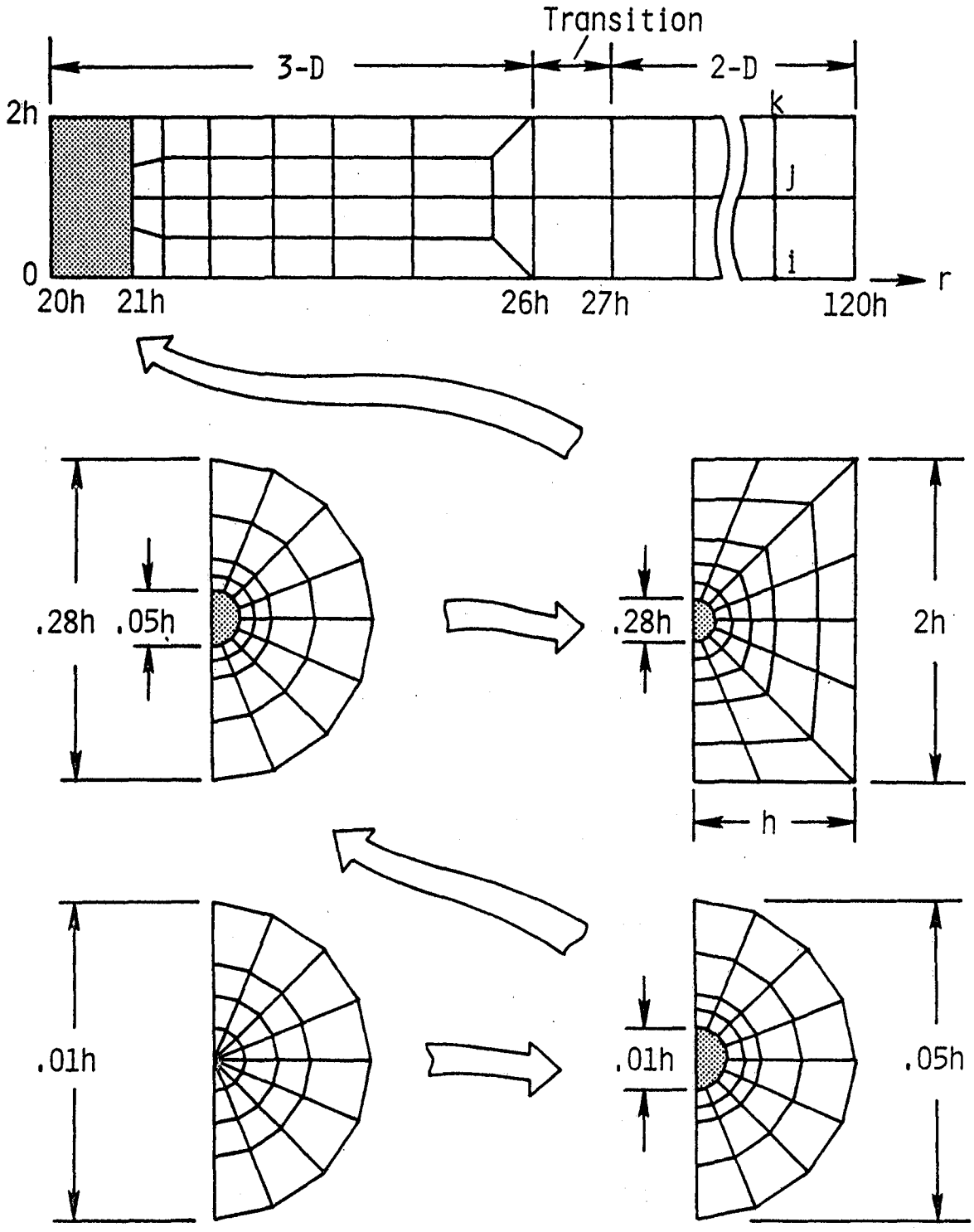

Figure 3.- Finite-element mesh for θ = constant planes.

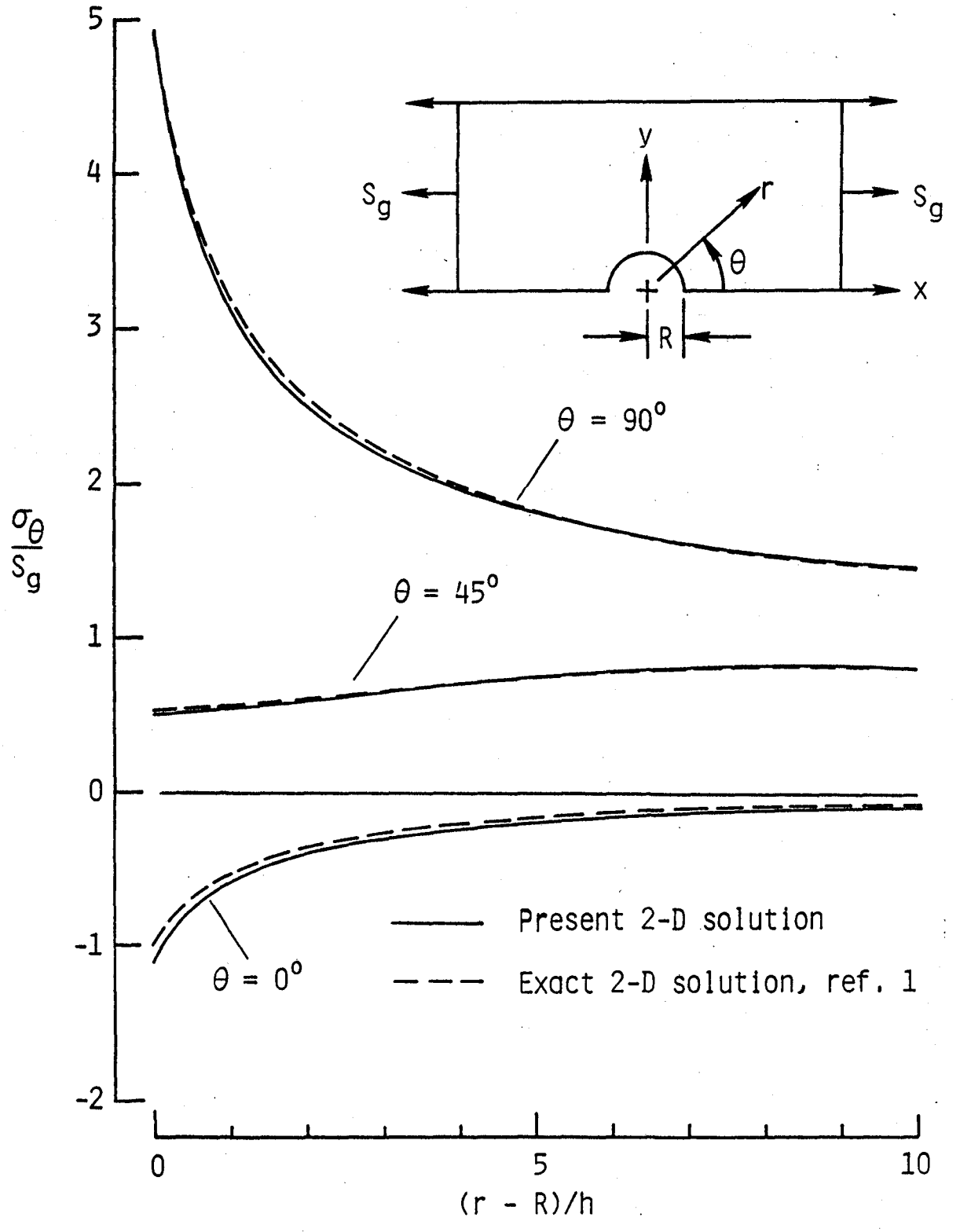

Figure 4.- σ_θ distributions from 2-D analyses of 0/90 laminate.

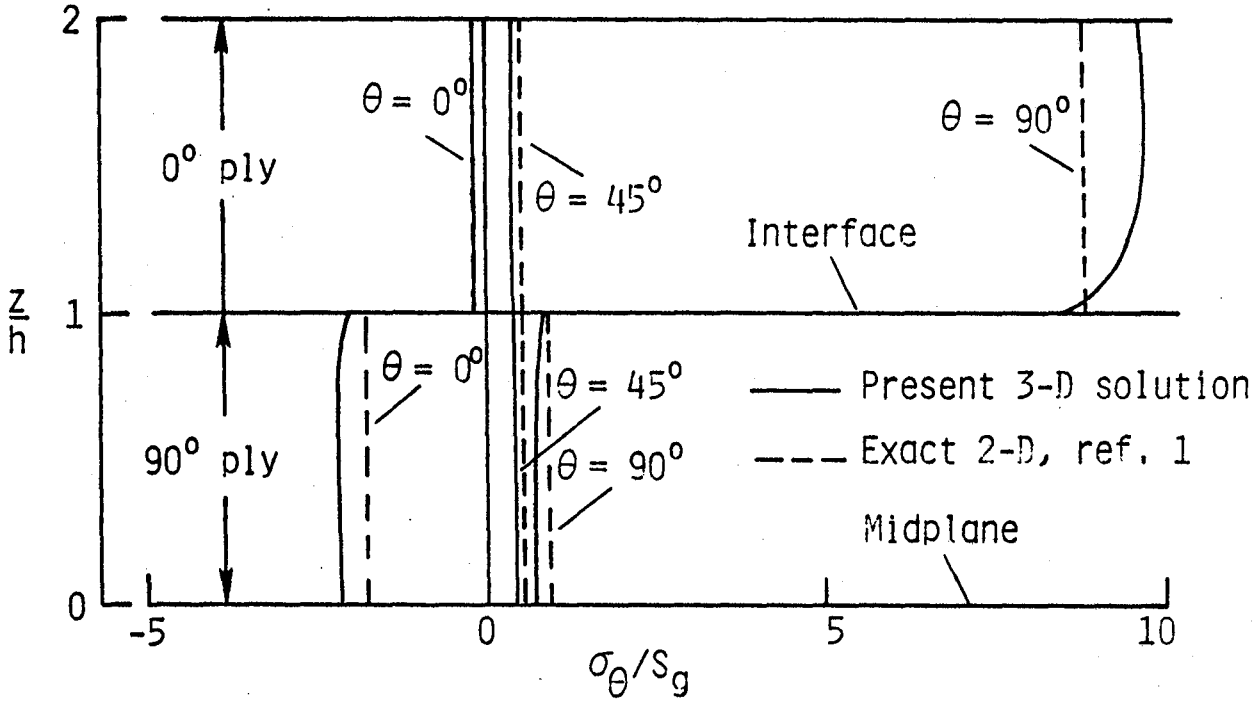

(a) $[0/90]_s$ laminate.

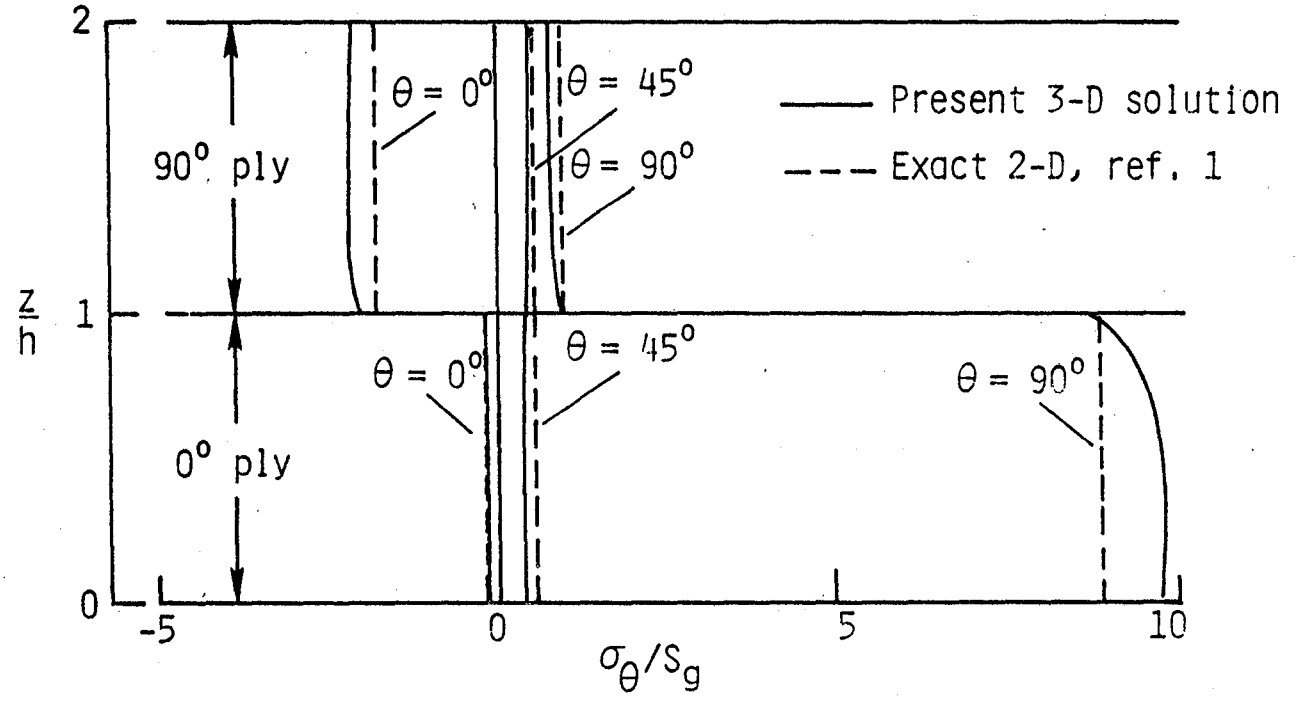

(b) $[90/0]_s$ laminate.

Figure 5.- $\sigma_{\theta\theta}$ distributions through the laminate thickness at the hole boundary (r/R = 1).

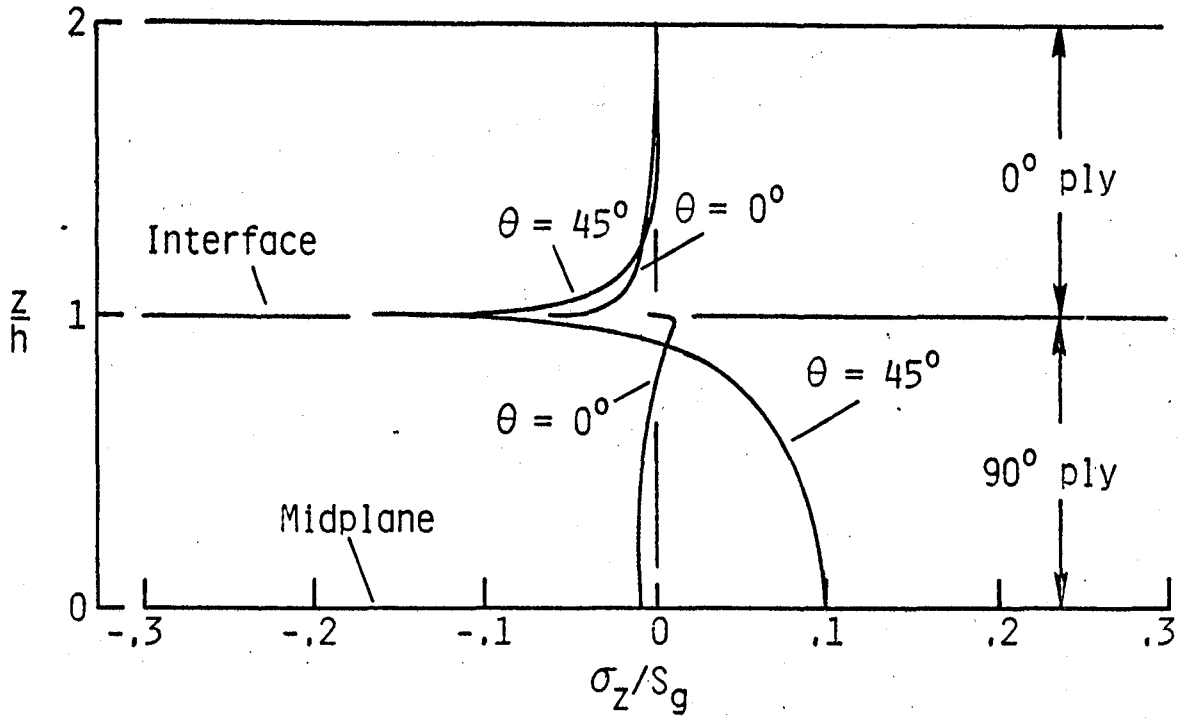

(a) $\theta = 0^\circ$ and 45° in $[0/90]_s$ laminate.

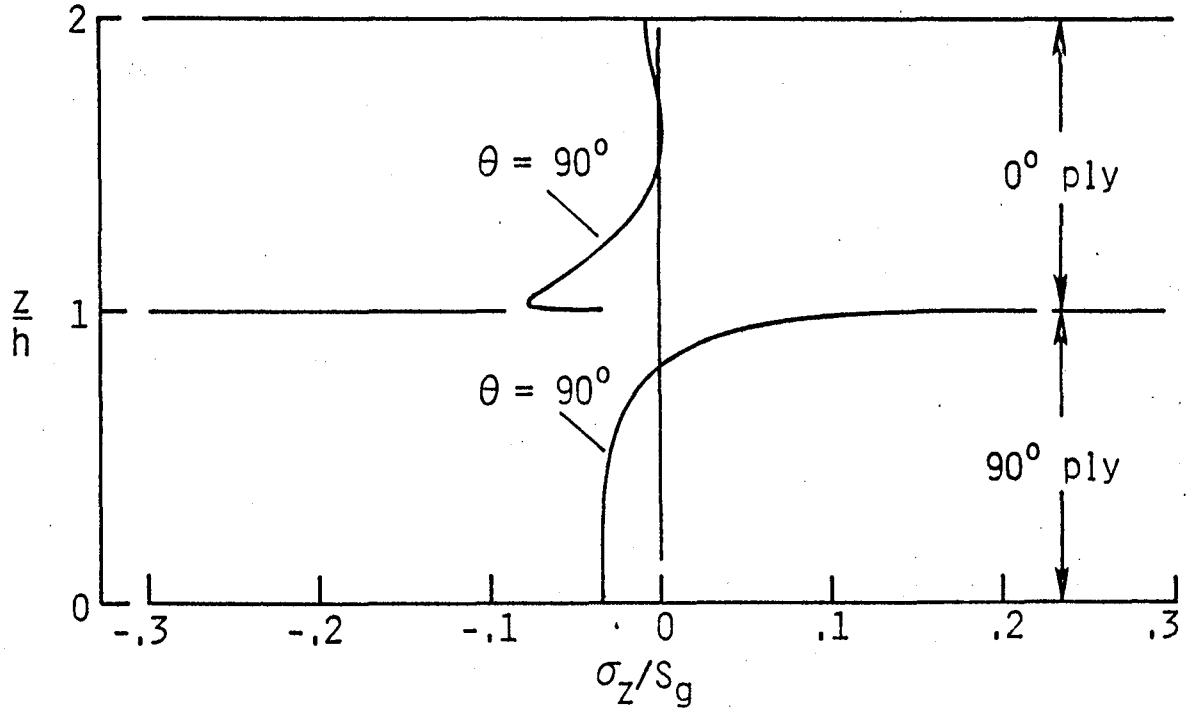

(b) $\theta = 90^\circ$ in $[0/90]_s$ laminate.

Figure 6.- σ_z distributions through the laminate thickness at the hole boundary (r/R = 1).

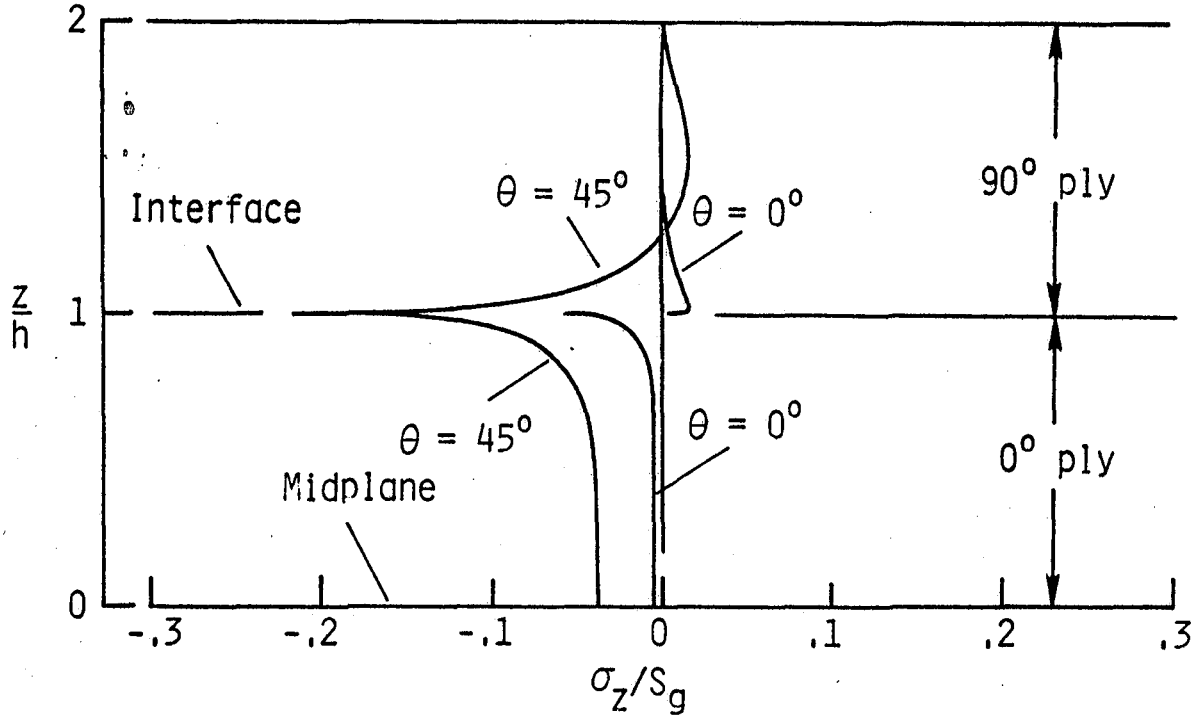

(c) $\theta = 0^\circ$ and 45° in $[90/0]_s$ laminate.

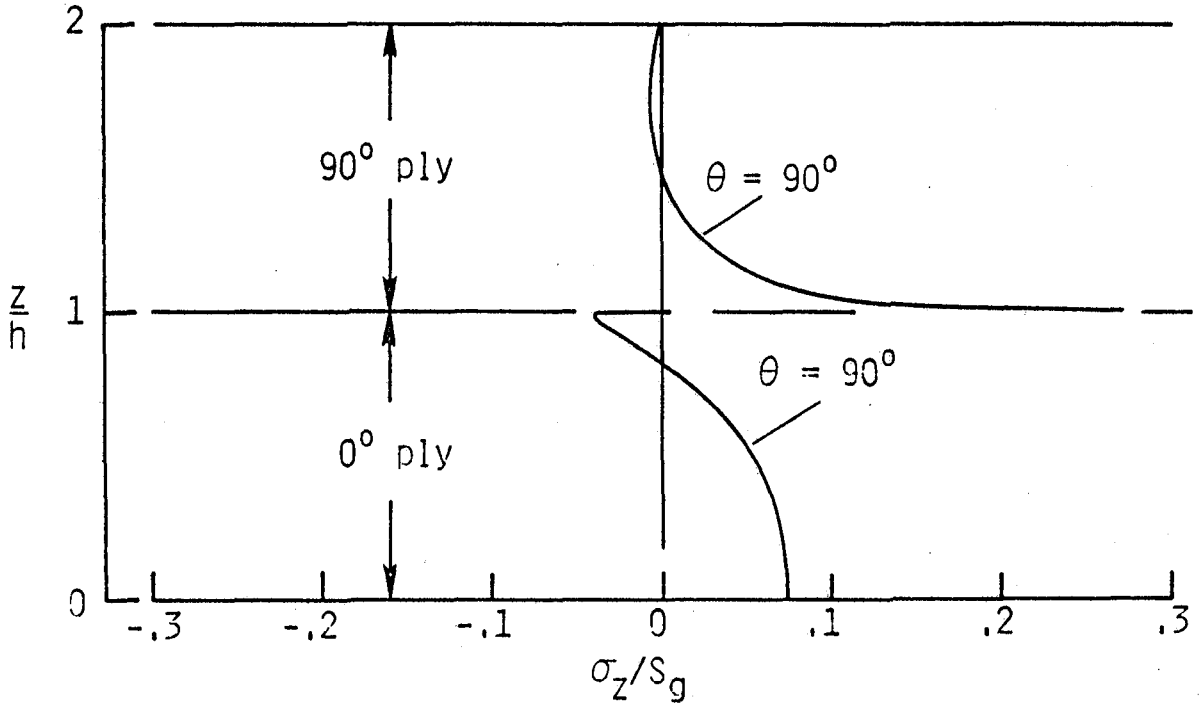

(d) $\theta = 90^\circ$ in $[90/0]_s$ laminate.

Figure 6.- Concluded.

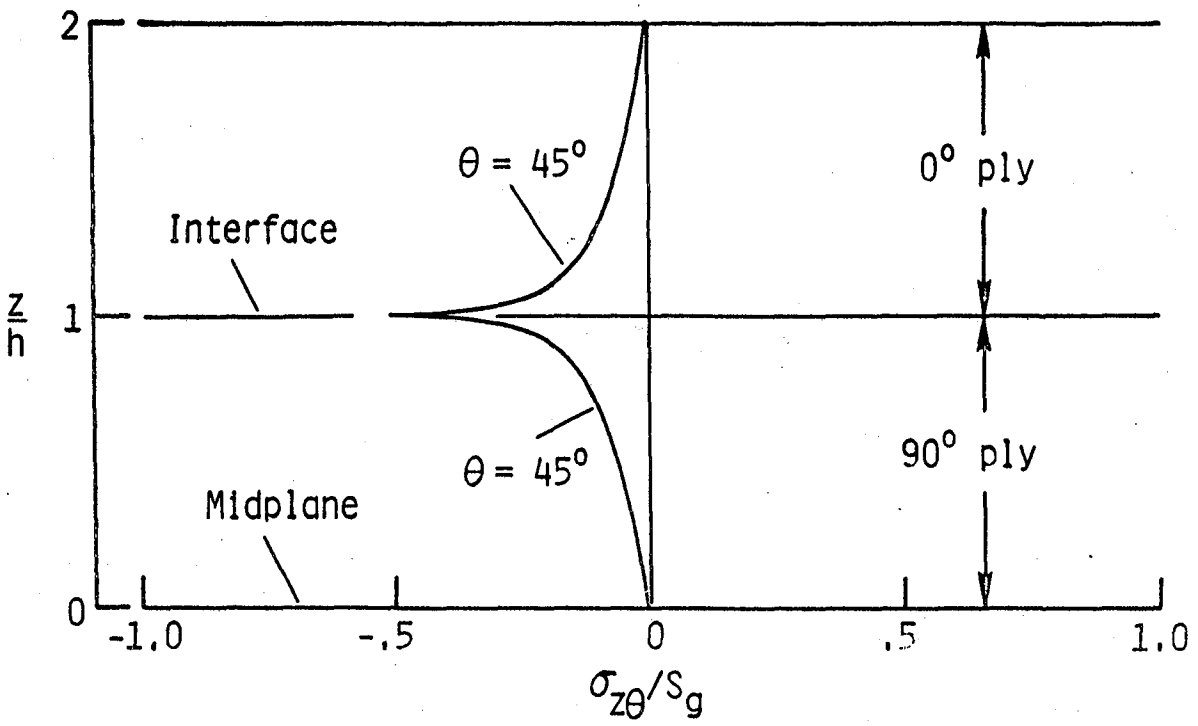

(a) $[0/90]_s$ laminate.

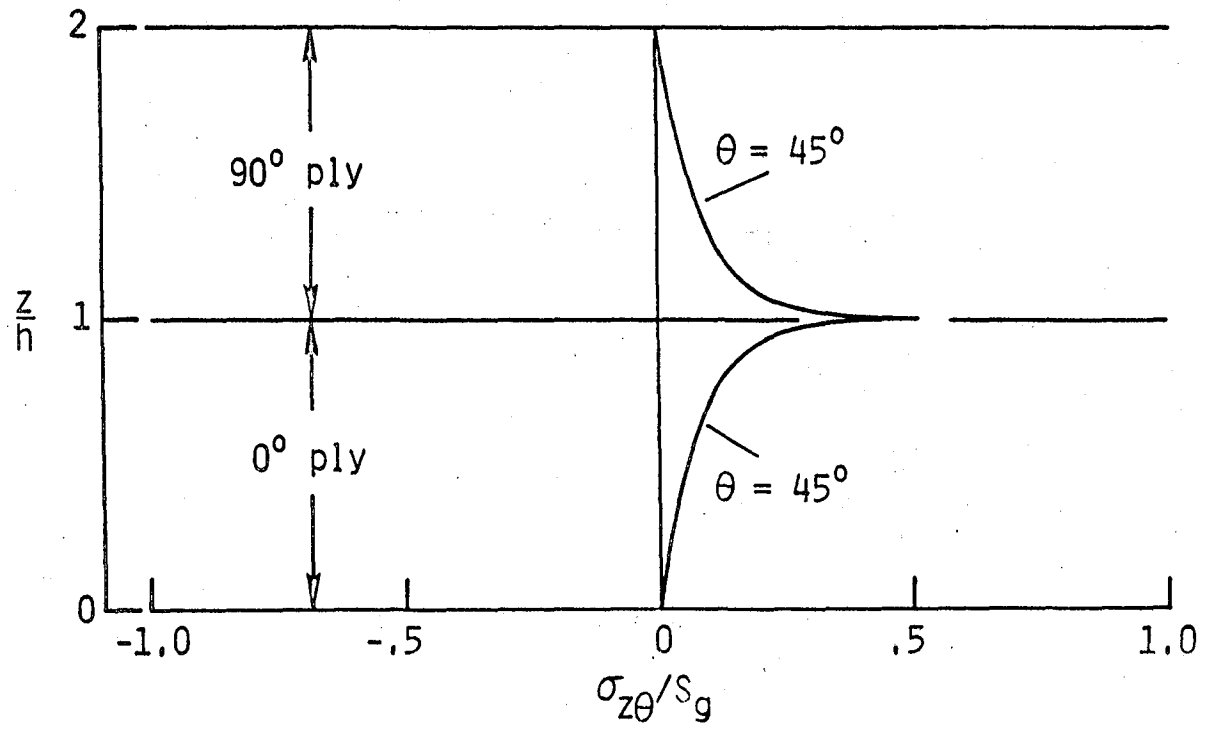

(b) $[90/0]_s$ laminate.

Figure 7.- $\sigma_{z\theta}$ distributions through the laminate thickness at the hole boundary (r/R = 1).

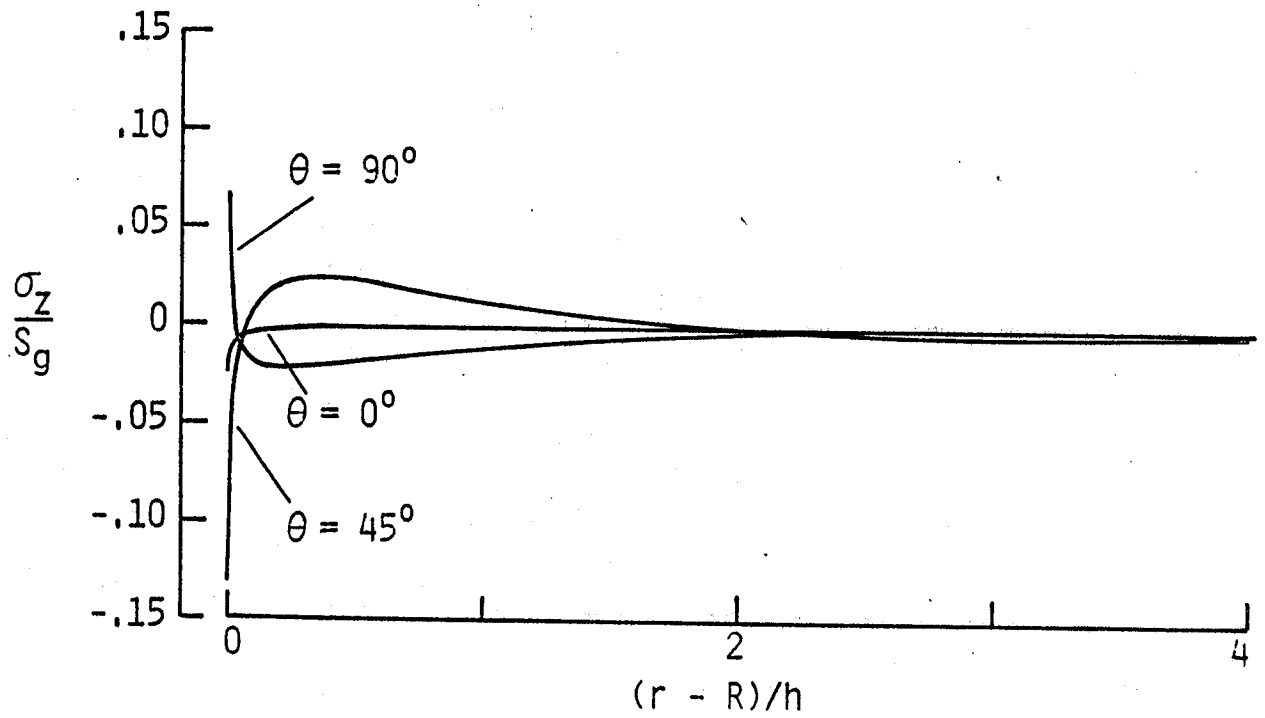

(a) $[0/90]_s$ laminate.

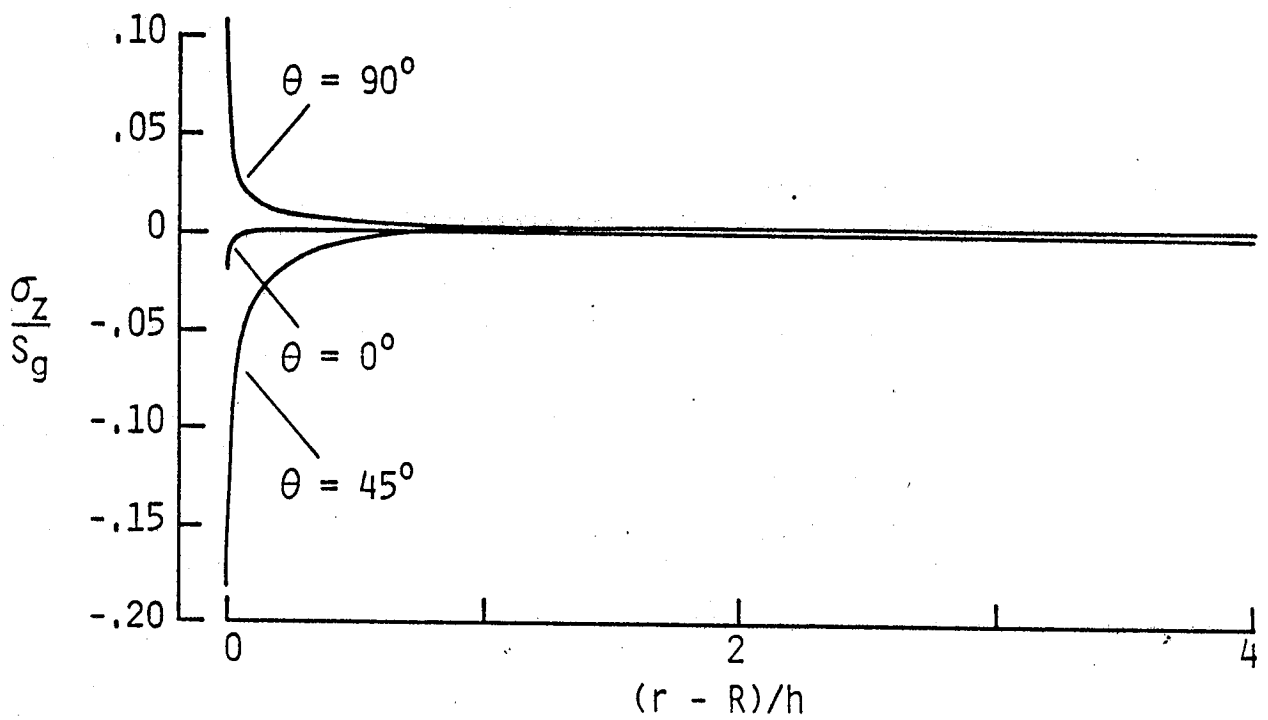

(b) $[90/0]_s$ laminate.

Figure 8.- σ_z radial distributions at the ply interface (z = h).

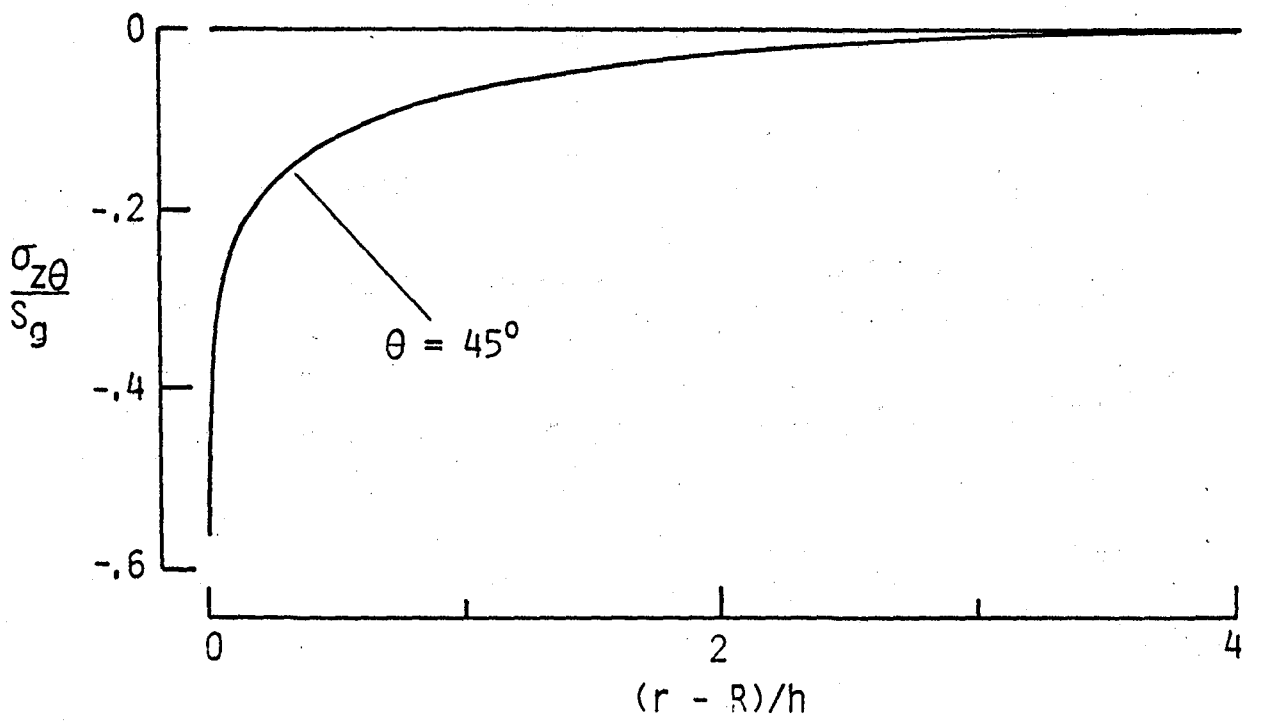

(a) $[0/90]_s$ laminate.

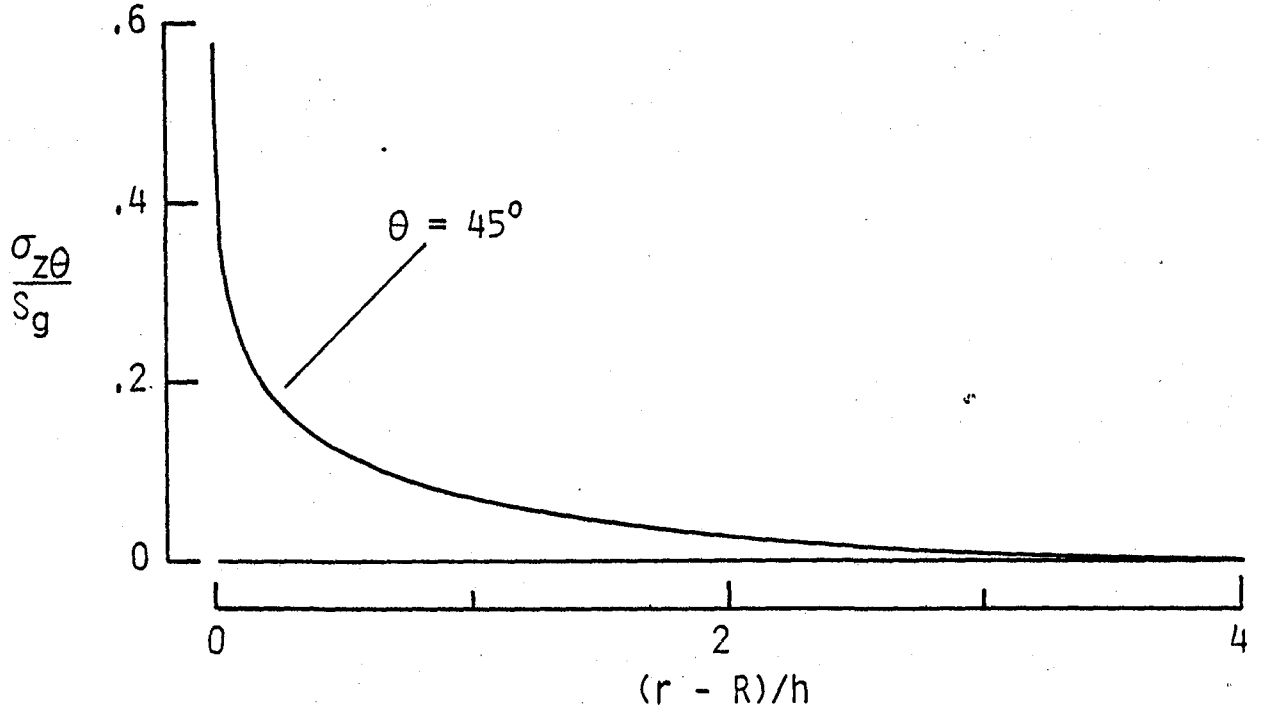

(b) $[90/0]_s$ laminate.

Figure 9.- $\sigma_{z\theta}$ radial distributions at the ply interface (z = h).

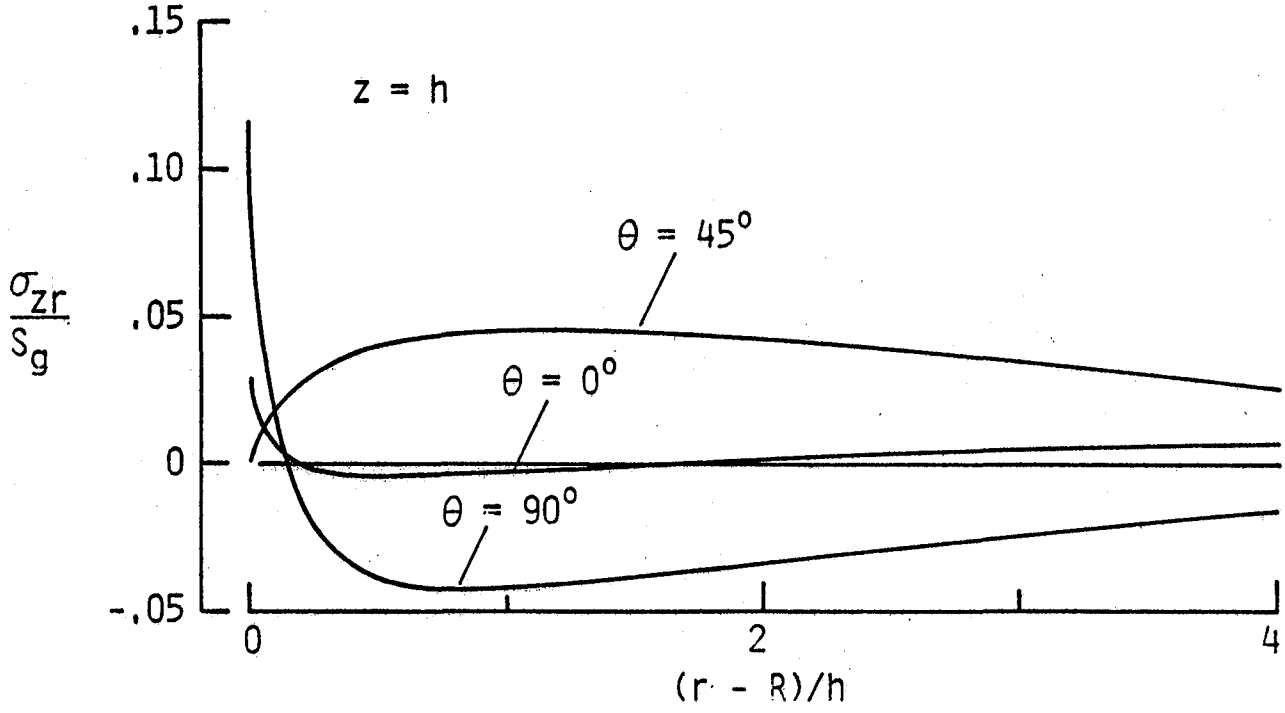

(a) $[0/90]_s$ laminate.

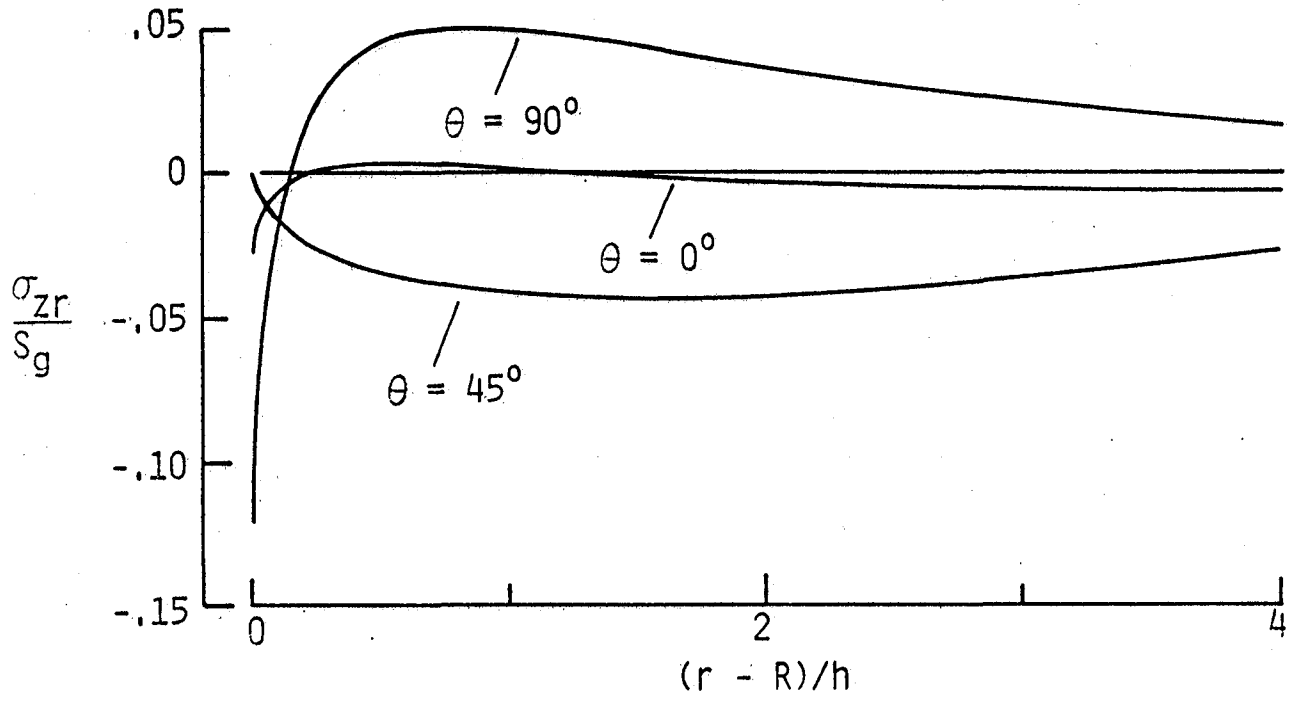

(b) $[90/0]_s$ laminate.

Figure 10.- σ_{zr} radial distributions at the ply interface (z = h).

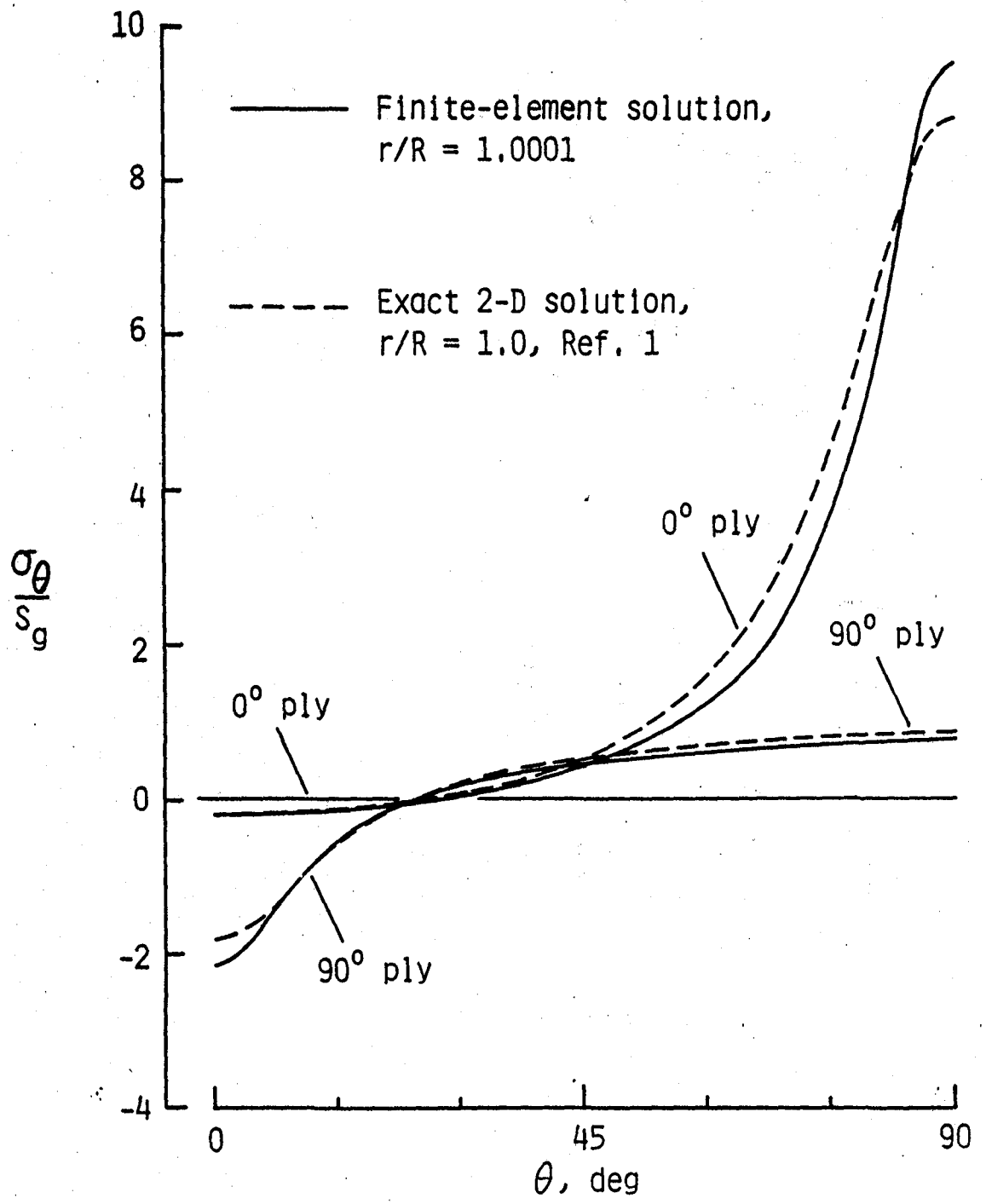

Figure 11.- $\sigma_{\theta\theta}$ distributions around hole (at the ply interface, z = h).

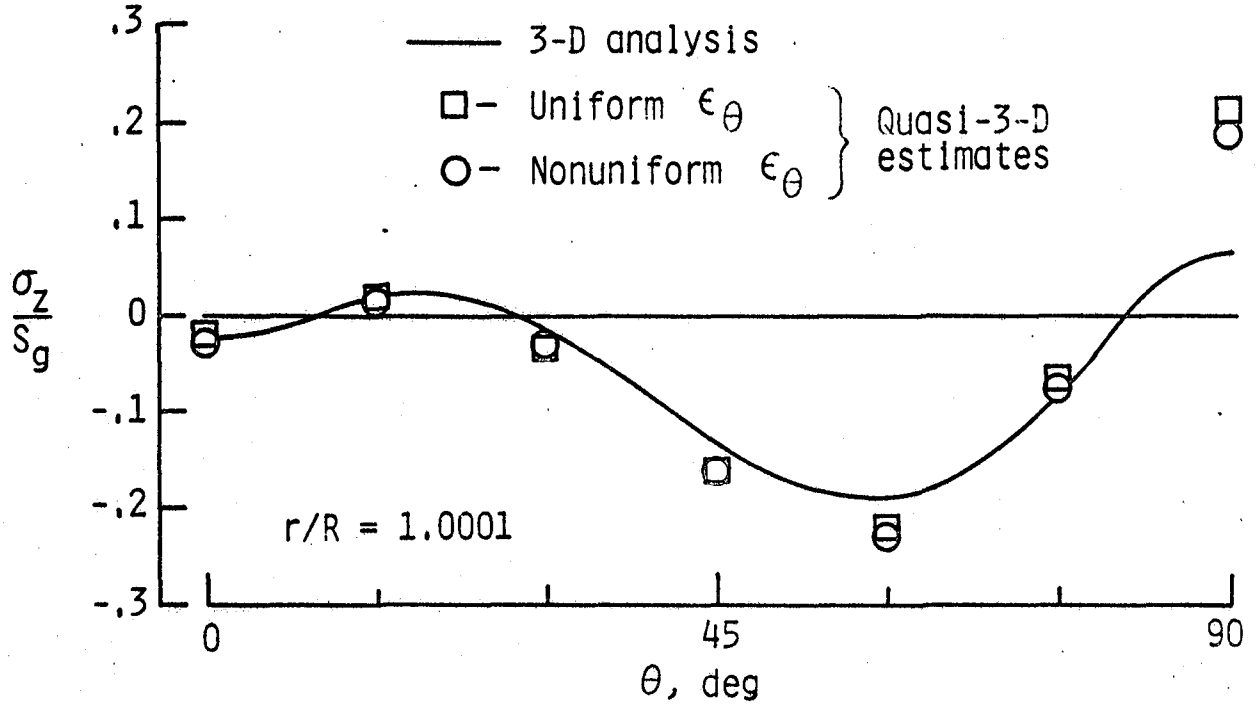

(a) $[0/90]_s$ laminate.

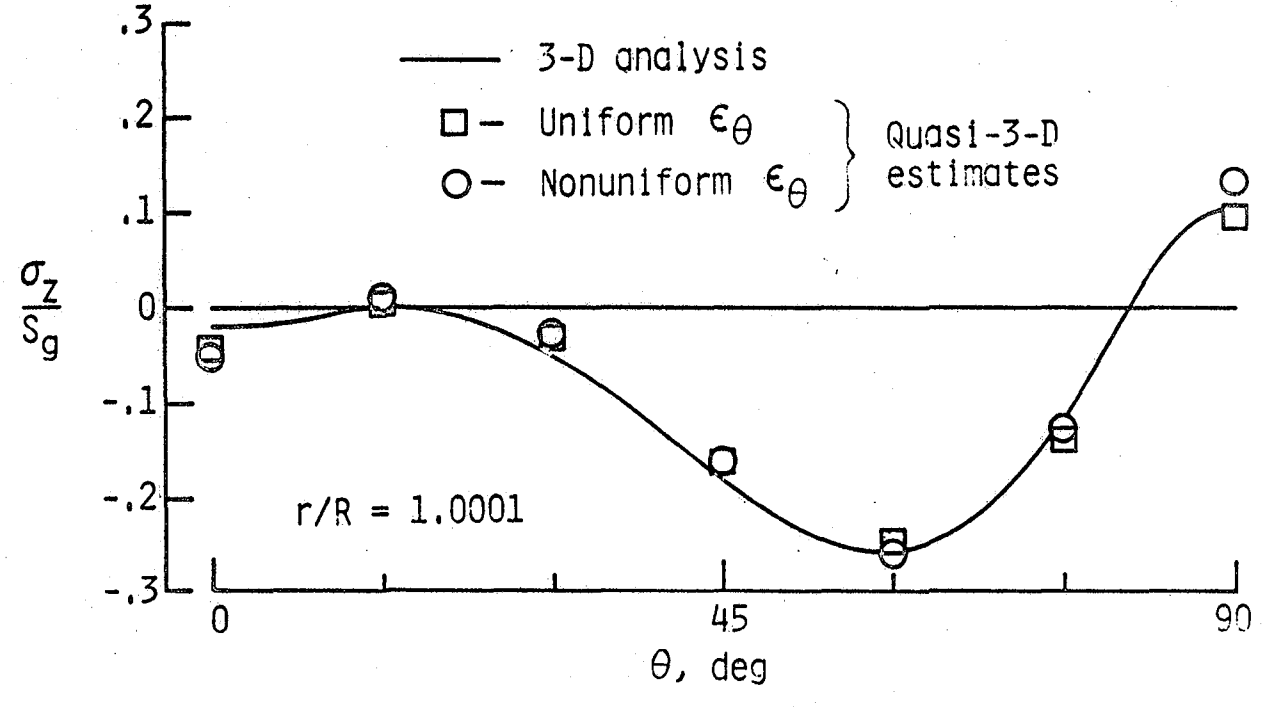

(b) $[90/0]_s$ laminate.

Figure 12.- σ_z distributions around hole (at the ply interface, z = h).

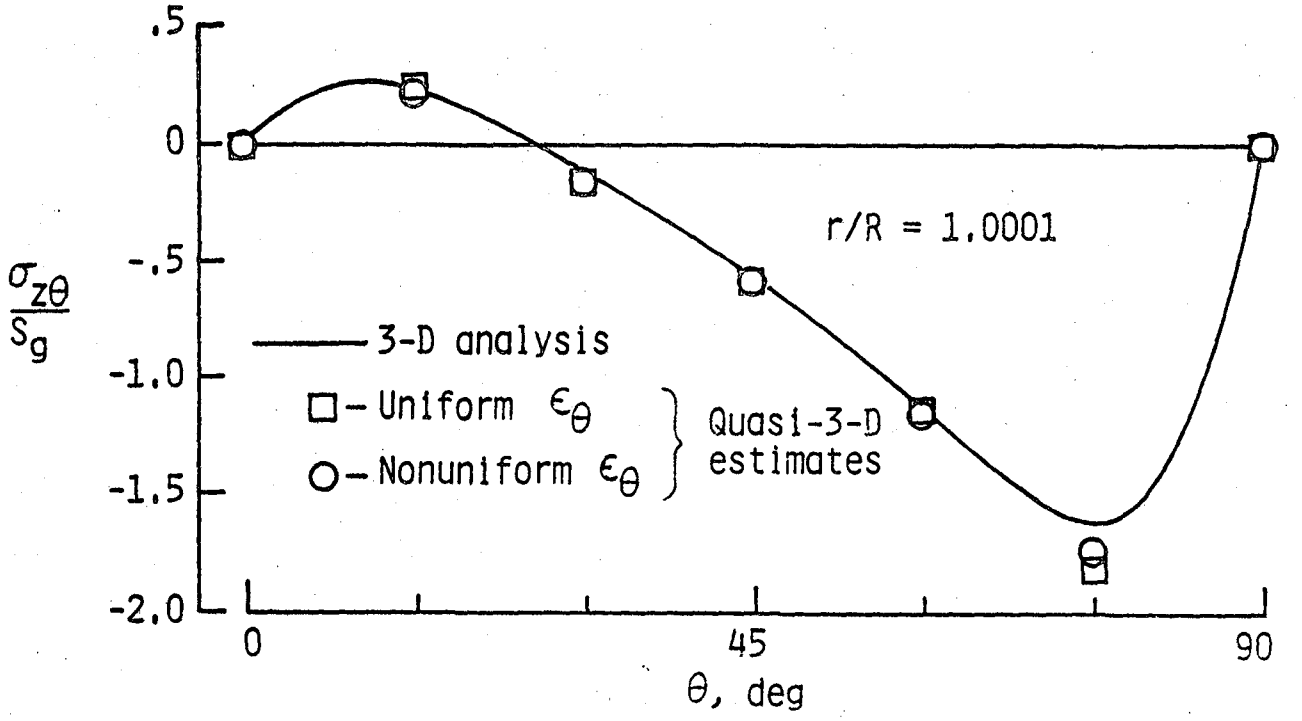

(a) $[0/90]_s$ laminate.

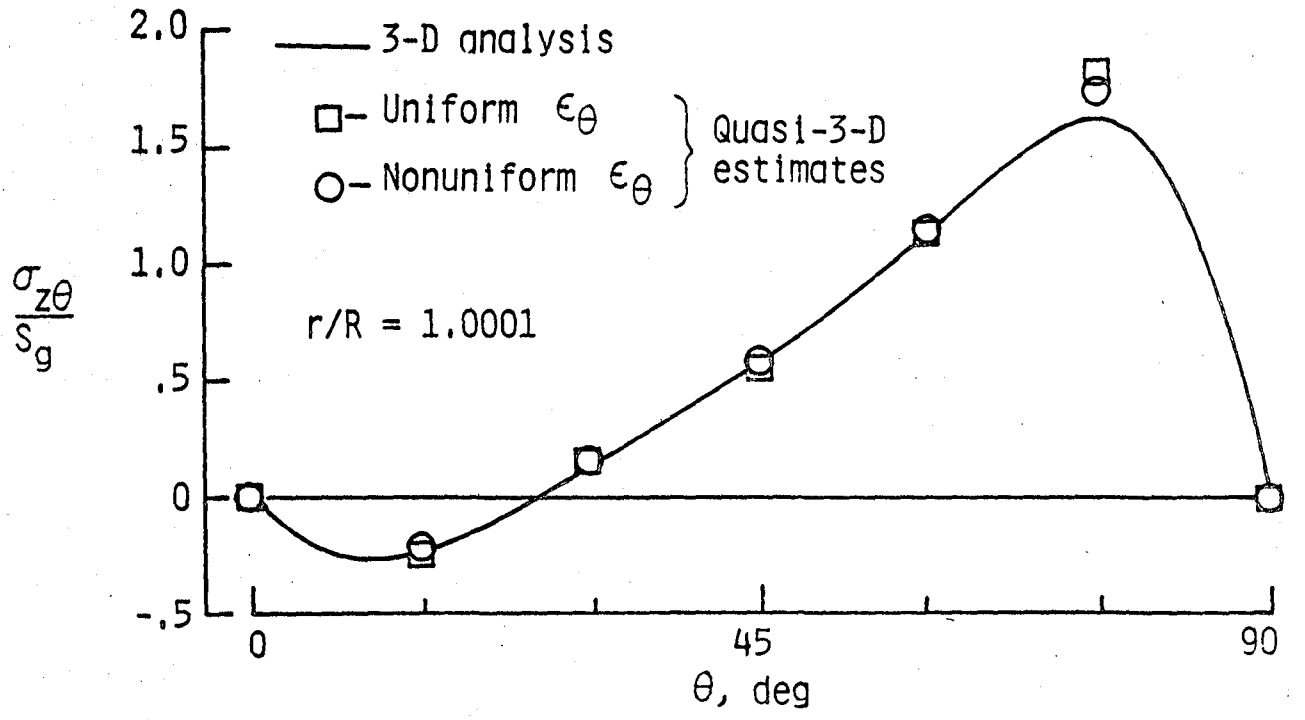

(b) $[90/0]_s$ laminate.

Figure 13.- $\sigma_{z\theta}$ distributions around hole (at the ply interface, z = h).

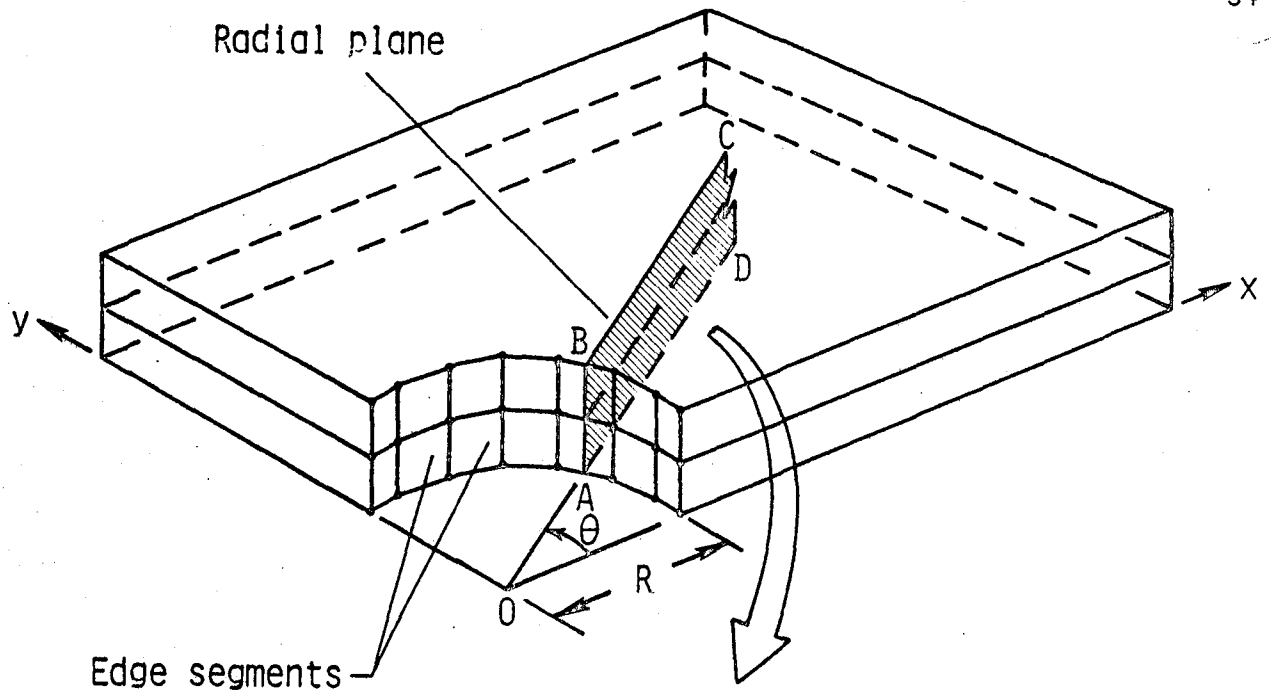

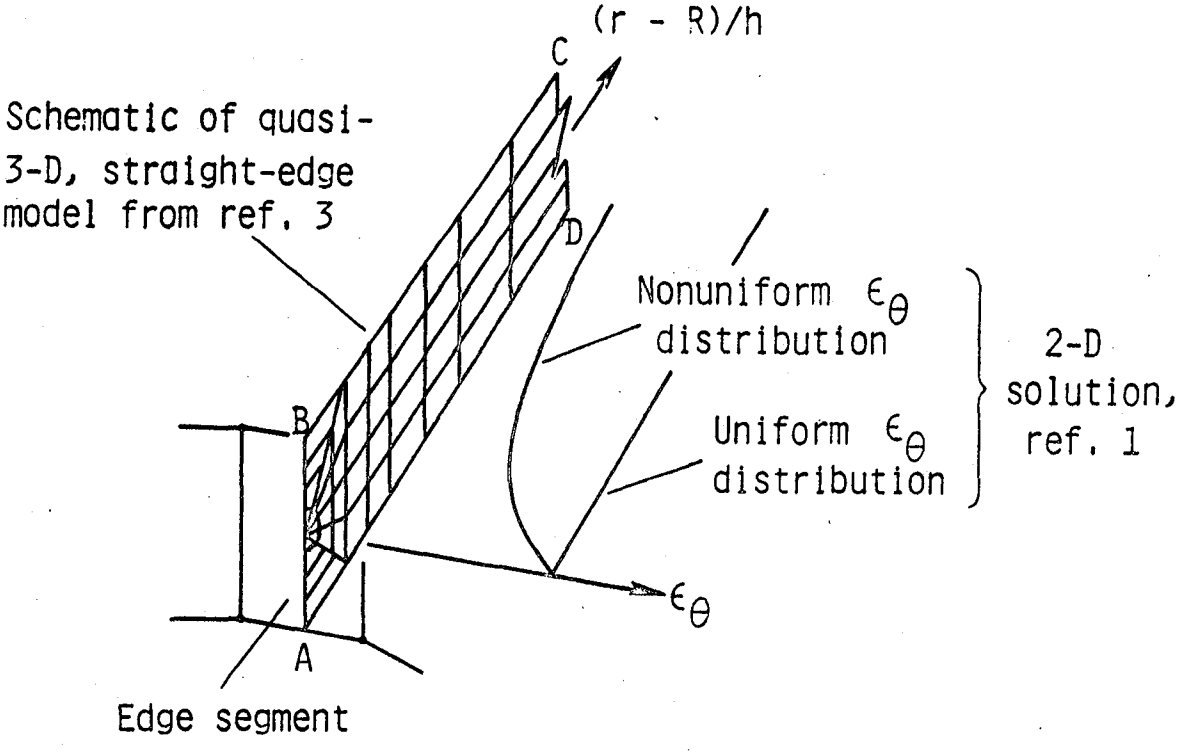

Figure 14.- Straight-edge approximation for quasi-3-D analysis of laminate hole.

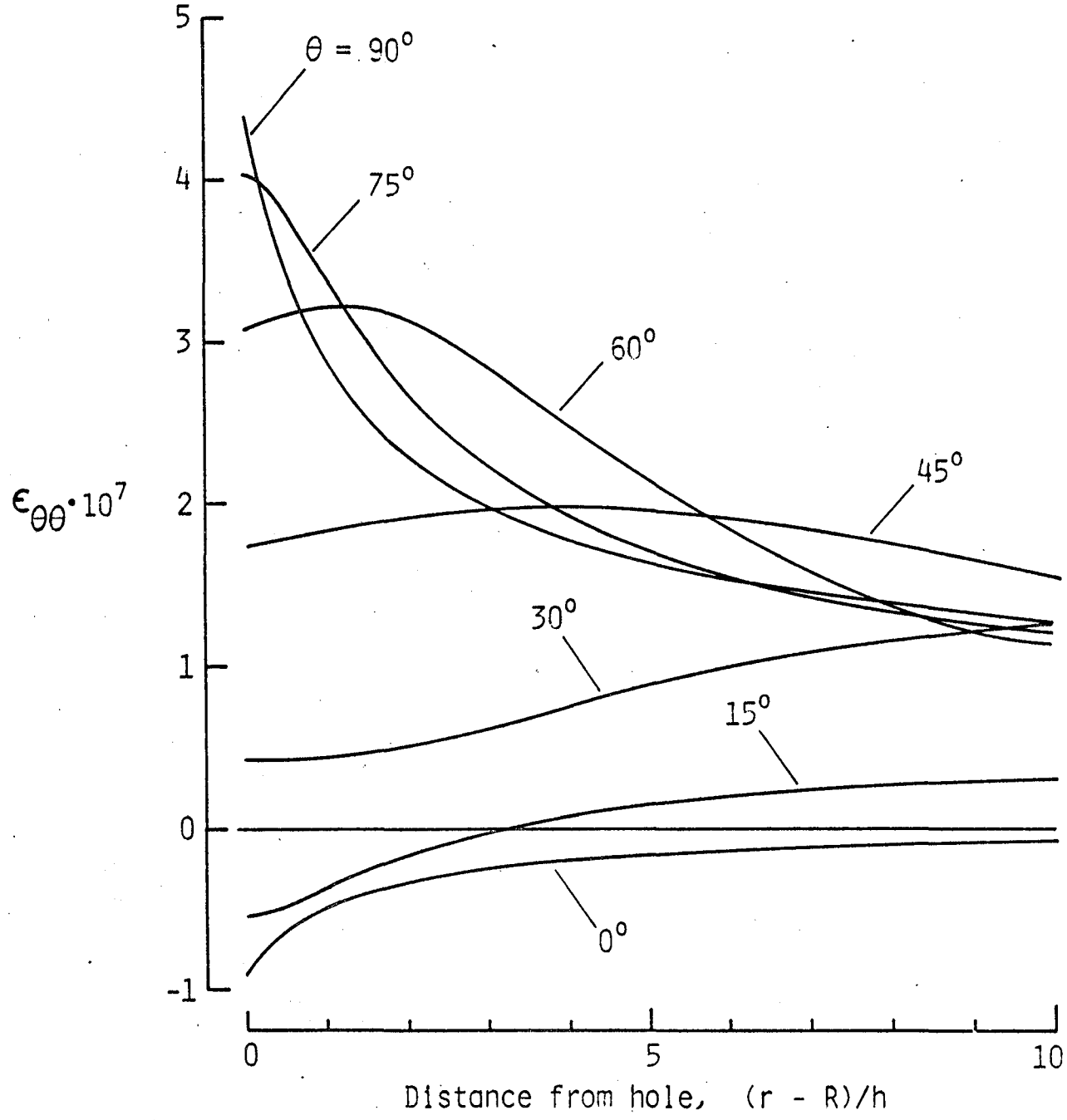

Figure 15.- $\epsilon_{\theta\theta}$ strain distributions from exact 2-D analysis, $S_g = 1$, ref. 1.

1. Report No.	2. Government Accession No.	3. Recipient's Catalog No.
NASA TM-83300		

4. Title and Subtitle	5. Report Date
THREE-DIMENSIONAL ANALYSIS OF $[0/90]_s$ AND $[90/0]_s$ LAMINATES WITH A CENTRAL CIRCULAR HOLE	April 1982
	6. Performing Organization Code 505-33-23-02

7. Author(s)	8. Performing Organization Report No.
Ivatury S. Raju and John H. Crews, Jr.	
	10. Work Unit No.
9. Performing Organization Name and Address	
NASA Langley Research Center Hampton, VA 23665	11. Contract or Grant No.
	13. Type of Report and Period Covered
12. Sponsoring Agency Name and Address	Technical Memorandum
National Aeronautics and Space Administration Washington, DC 20546	14. Army Project No.

15. Supplementary Notes

This paper has been accepted for publication in Composites Technology Review.

16. Abstract

Stress distributions were calculated near a circular hole in $[0/90]_s$ and $[90/0]_s$ laminates, using a three-dimensional finite-element analysis. These stress distributions were presented three ways: through the thickness at the hole boundary, along radial lines at the 0/90 and 90/0 interfaces, and around the hole at these interfaces. The interlaminar normal stress, σ_z, and the shear stress, $\sigma_{z\theta}$, distributions had very steep gradients near the hole boundary, suggesting interlaminar stress singularities. The largest compressive σ_z stress occurred at about 60° from the load axis; the largest occurred near 75°. A simple procedure was introduced to calculate interlaminar stresses near the hole boundary. It used stresses calculated by an exact two-dimensional analysis of a laminate with a hole as input to a quasi-three-dimensional model. It produced stresses that agreed closely with those from the three-dimensional finite-element model. For laminates with holes, this simple procedure may become a viable alternative to three-dimensional finite-element analyses.

17. Key Words (Suggested by Author(s))	18. Distribution Statement
Laminated composites Circular hole 3-D finite-element analysis Interlaminar stresses Edge stresses	Unclassified - Unlimited Subject Category 24

19. Security Classif. (of this report)	20. Security Classif. (of this page)	21. No. of Pages	22. Price*
Unclassified	Unclassified	36	A03

*For sale by the National Technical Information Service, Springfield, Virginia 22161

LIBRARY MATERIAL SLIP

DO NOT REMOVE SLIP FROM MATERIAL

Delete your name from this slip when returning material to the library.

NAME	DATE	MS
~~Walker, S.~~	~~10/26/00~~	~~396~~

NASA Langley Form 474 (Rev. Oct. 1999)